Podoplanin function is switched by partner proteins on fibroblastic reticular cells

Charlotte M. de Winde[1], Spyridon Makris[1*], Lindsey Millward[1*], Agnesska C. Benjamin[1], Giulia Cazzagon[1], Victor G. Martinez[1], and Sophie E. Acton[1,✉]

[1]Stromal Immunology Group, MRC Laboratory for Molecular Cell Biology, University College London, Gower Street, London, WC1E 6BT, United Kingdom
[*]These authors contributed equally

Lymph node expansion is pivotal during immune activation. It is controlled by interactions between CLEC-2^{hi} migratory dendritic cells and podoplanin^{+} fibroblastic reticular cells (FRCs) resulting in rapid loss of actomyosin contractility permitting FRC spreading. Podoplanin is an inflammatory marker in many pathologies, reported to facilitate both contractility and cell protrusions. However, how podoplanin expression is regulated, and how this one membrane protein can elicit these opposing phenotypes is unknown. We report that CLEC-2 binding to FRCs induces transcriptional upregulation of podoplanin, increasing surface protein expression. Further, we find that tetraspanin CD82 is required for trafficking of podoplanin to the plasma membrane. At the cell surface, podoplanin elicits multiple functions, balanced by its membrane binding partners hyaluronan receptor CD44 and tetraspanin CD9. FRCs lacking expression of both CD44 and CD9 are hypercontractile, and upon binding to CLEC-2^{hi} dendritic cells, both CD44 KO and CD9 KO FRCs exhibit defective protrusion formation and fail to spread. Podoplanin co-localises with CD44 or CD9 in distinct membrane domains, and both CD44 and CD9 are required for FRCs to spread in response to dendritic cells, however they control formation of cell protrusions via different and complimentary mechanisms. *In vivo*, surface expression levels of podoplanin, CD44 and CD9 are upregulated on T-cell zone FRCs in the early phase of lymph node expansion. Our data support a model whereby podoplanin resides in distinct plasma membrane domains, and that CLEC-2 binding serves as a molecular switch to change podoplanin function.

Podoplanin | CD44 | CD9 | CD82 | Tetraspanins | Fibroblastic reticular cell | Lymph node

Correspondence: ***s.acton@ucl.ac.uk***

Introduction

Podoplanin was discovered almost simultaneously in a wide variety of tissues and cell types, and has therefore been assigned multiple names (podoplanin, gp38, Aggrus, PA2.26, D2-40, T1α) based on its function in different contexts (1). This type I transmembrane mucin-like glycoprotein is expressed on the surface of kidney podocytes, osteocytes, glial cells, type I alveolar cells, skin keratinocytes, lymphatic endothelial cells (LECs), and some fibroblast subsets (2–9). Podoplanin plays a pivotal role in the correct development of heart, lungs, secondary lymphoid tissues and lymphatic vasculature. Podoplanin *null* mice exhibit embryonic lethality due to cardiovascular problems or die shortly after birth of respiratory failure (10–12), and exhibit defective blood-lymphatic vasculature separation (13, 14), so understanding the full range of podoplanin functions in other tissues has been challenging.

Podoplanin expression levels are dynamic through development and in pathological conditions. Upon wounding, epidermal keratinocytes increase podoplanin expression (15), and in sepsis, inflammatory macrophages express podoplanin (16). In many types of cancer, podoplanin is upregulated both on tumour cells and on cancer-associated fibroblasts (CAFs) in the tumour microenvironment (1, 17). In homeostasis, lymph nodes express high levels of endogenous podoplanin (7), which increases upon *in vivo* immunization (18). Interestingly, follicular lymphoma-bearing lymph nodes show decreased podoplanin expression (19). The molecular mechanisms controlling these changes in podoplanin expression are not fully understood. In skin, brain and bone tumour cells, the podoplanin gene *Pdpn* is under control of the transcription factor activator protein 1 (AP-1) (20–22), but in LECs, *Pdpn* is expressed under the control of *Prox1* (23). It is therefore likely that podoplanin expression can be regulated by multiple signalling pathways depending on cell type, tissue context and inflammatory cues.

Podoplanin activity is involved in many different cell phenotypes and functions. In fibroblastic reticular cells (FRCs), podoplanin drives actomyosin contractility and controls cell stiffness through ERM binding (24, 25). Upon initiation of an immune response, CLEC-2^{hi} migratory dendritic cells bind podoplanin on FRCs inhibiting actomyosin contractility, resulting in FRC spreading and elongation for rapid lymph node expansion (24, 25). Furthermore, podoplanin expression by FRCs is essential for lymph node development, and FRC function can also be altered by binding of CLEC-2-expressing platelets (26, 27). In LECs, podoplanin binding to galectin-8 supports adhesion to the extracellular matrix (28), whereas in epidermal keratinocytes, podoplanin expression is inversely correlated with β1 integrin-mediated adhesion (29). Further studies have focused on the role of podoplanin in cell motility. In mesenchymal stromal cells, it has been shown that podoplanin expression is required for Rac1-dependent migration (30). Furthermore, podoplanin drives cell migration of CAFs (31) and cancer cells (32, 33), and as such plays a role in several stages of the metastasis process (1). Podoplanin is expressed at the invasive front of tumours (34), and more specifically recruited to the adhesion ring of invadopodia where it localizes in lipid rafts (35). In addition, podoplanin-dependent regulation of ezrin and moesin

activates RhoA, driving epithelial-to-mesenchymal transition (36). We ask what molecular mechanisms permit one membrane protein to drive these varied and sometimes contradictory phenotypes.

Since podoplanin has a very short cytoplasmic tail consisting of only nine amino acids (37), it is suggested that podoplanin would require binding partners to execute its diverse range of functions. Many binding partners have already been identified (1, 17), but their functions have mainly been described in the context of podoplanin upregulation in cancer. In this study, we seek to understand the function of endogenous podoplanin-binding partner interactions on FRCs in the normal physiology of immune responses.

Tetraspanins and interacting membrane proteins can link extracellular cues to intracellular signalling. Tetraspanins are a superfamily of four-transmembrane proteins that form tetraspanin-enriched microdomains via interactions with each other and binding partners. These microdomains spatially organize the plasma membrane into a tetraspanin web, which facilitates cellular communication (38, 39). We studied the role of two known podoplanin membrane binding partners in regulating FRC function: the hyaluronan receptor CD44 (33) and tetraspanin CD9 (40). The interaction of podoplanin with CD9 is mediated by CD9 transmembrane domains 1 and 2, and this interaction impairs cancer metastasis by inhibiting platelet aggregation (40). In contrast, the podoplanin/CD44 interaction at tumour cell protrusions promotes cancer cell migration (33). In NIH/3T3 fibroblasts, co-expression of CD44 and podoplanin reversed the hypercontractile phenotype seen in cells overexpressing podoplanin (24), suggesting an inhibitory function for CD44 in driving actomyosin contractility in fibroblasts. It has previously been shown that podoplanin and CD44 both reside in lipid rafts on MDCK cells (41). CLEC-2 binding to FRCs drives podoplanin clustering into cholesterol-rich domains (24), but the function of these podoplanin clusters is unknown.

Here, we report that podoplanin expression increases upon CLEC-2 binding and that membrane binding partners CD44 and CD9 both stabilise podoplanin surface levels, and temper hypercontractility. Binding of CLEC-2 serves as a molecular switch to change podoplanin function, reducing actomyosin contractility and inducing FRC spreading. CD44 and CD9 both contribute to FRC spreading by balancing lamellipodia and filopodia-like cell protrusions, respectively. And both CD44 and CD9 expression is increased on T-cell zone FRCs during early phases of lymph node expansion when FRC spreading is observed (24, 25).

Results

Podoplanin expression is upregulated upon CLEC-2 stimulation. Podoplanin expression can be induced following injury or inflammation (6, 8). During an immune response, endogenous podoplanin levels on FRCs in lymph nodes have been reported to increase (18, 25, 42), but it is unknown how this is regulated. In tissue sections, we observe a clear increase in podoplanin expression on the lymph node FRC network 6 days after *in vivo* immunization (Fig. 1a). Since FRCs in the initial phase of an immune response show loss of actomyosin contractility to allow spreading of the FRC network (24), we hypothesize that these cytoskeletal changes can also drive increased podoplanin expression. We inhibit actomyosin contractility by treating FRCs with Rho-kinase (ROCK) inhibitor Y-27632. However, ROCK inhibition decreases podoplanin surface expression on lymph node-derived primary FRCs (CD140α^+CD31$^-$/PDGFRα^+PECAM-1$^-$; Fig. 1b-c).

In vivo, loss of actomyosin contractility in FRCs is driven by CLEC-2^{hi} migratory dendritic cells which arrive in the lymph node in the first days after immunization (24). Therefore, we next investigate if CLEC-2 binding increases podoplanin expression in FRCs. To model the prolonged CLEC-2 exposure by migratory dendritic cells coming into the lymph node over several days (24), we generated a CLEC-2-Fc-secreting FRC cell line (43). CLEC-2-stimulated FRCs show increased podoplanin surface expression compared to control FRCs (Fig. 1d; flow cytometry results not shown), which cannot be explained solely by stabilisation of podoplanin at the plasma membrane, as total podoplanin protein levels are also increased (Fig. 1e). This suggests that regulation of podoplanin occurs at the transcriptional level, and indeed we find that *Pdpn* mRNA levels are 4-fold higher in CLEC-2-stimulated FRCs compared to controls (Fig. 1f). Overexpression of podoplanin drives hypercontractility in fibroblast cell lines (24), yet these data show that podoplanin expression is increased during the initiation of lymph node expansion, when FRCs are elongating and spreading. This suggests that in FRCs, high podoplanin levels are effectively balanced to prevent hypercontractility. Furthermore, these data indicate that the increased levels of podoplanin protein may be diverted from contractile signalling pathways and have additional functions in FRCs.

Tetraspanin CD82 is required for podoplanin membrane expression. Our data shows a 4-fold increase in *Pdpn* mRNA, and 2-fold higher protein levels upon CLEC-2 stimulation (Fig. 1d-f). Protein surface expression can be controlled by intracellular trafficking, binding to membrane proteins for stabilisation, and by degradation. Tetraspanins are master-organisers of the plasma membrane, binding to and controlling expression of membrane proteins (38), but can also regulate protein trafficking (44). One candidate for controlling podoplanin expression is tetraspanin CD82 as it was recently reported that loss of CD82 in osteoclasts decreases podoplanin protein expression (45).

To investigate the function of CD82 in podoplanin expression in FRCs, we generated CD82 knock-out (KO) FRCs using CRISPR/Cas9 editing and selected single-cell clones by quantitative RT-PCR (Supplementary Fig. 1). Interestingly, CD82 KO FRCs almost completely lack podoplanin surface expression (Fig. 2a). To rule out an off-target effect of the CRISPR single guide RNA in the *Pdpn* gene, we generated CD82 KO clones in a podoplanin KO FRC cell line containing a doxycycline-inducible construct to re-express podoplanin. Interestingly, and in support of our original observations, FRCs lacking CD82 are also unable to express ex-

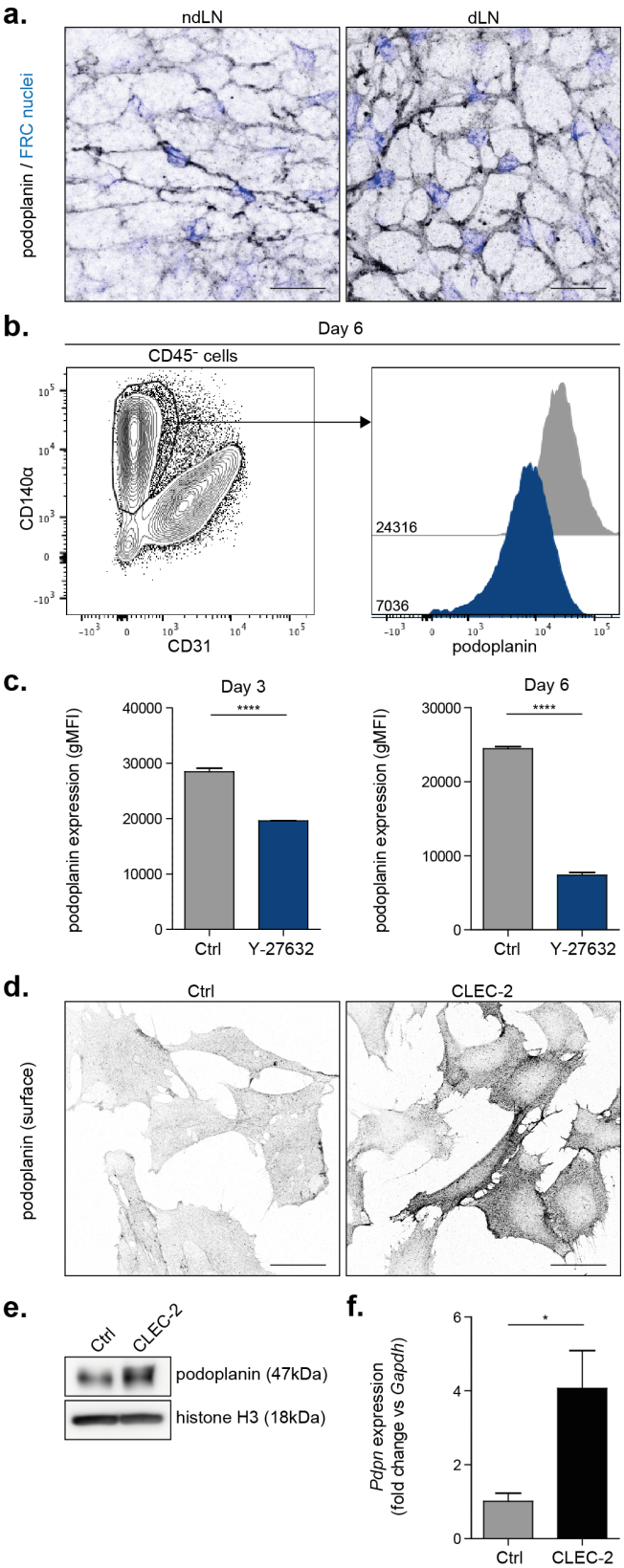

Fig. 1. Podoplanin expression on FRCs is increased in response to CLEC-2. a. Immunofluorescence of 10 microns thick cryosection of non-draining (nd; left) and draining (d; right) lymph nodes (LN) from PDGFR$\alpha^{H2B\text{-}GFP}$ mice immunized with CFA/OVA. Maximum Z stack projections of representative images are shown. The scale bars represent 20 microns. **b-c.** Cell suspensions of whole lymph nodes were cultured for 3 or 6 days with (blue) or without (grey) ROCK inhibitor (Y-27632). Podoplanin surface expression on FRCs (CD140α^+CD31$^-$) was measured using flow cytometry. Inguinal, branchial and axillary lymph nodes from 6 mice were pooled. n=3 replicates per condition per time point. ****p<0.0001, unpaired t-test, two-tailed. gMFI = geometric mean fluorescence intensity. **d.** Immunofluorescence of podoplanin surface expression on control (Ctrl) or CLEC-2-Fc-expressing FRC cell lines. Maximum Z stack projections of representative images are shown. The scale bars represent 50 microns. **e.** Western blot analysis of total podoplanin (PDPN) expression in Ctrl or CLEC-2-Fc-expressing FRC cell lines. Histone H3 was used as loading control. Data are shown from one representative experiment. **f.** Podoplanin (*Pdpn*) mRNA expression Ctrl (grey) or CLEC-2-Fc-expressing (black) FRCs. *Pdpn* expression is calculated as fold change of *Gapdh* expression. Data shown as mean+SD, n=2 independent experiments. *p<0.05, unpaired t-test, one-tailed.

ogenous podoplanin in this inducible system (Fig. 2b). Further, we transiently transfected control and CD82 KO FRCs with CFP-tagged podoplanin (PDPN-CFP; Fig. 2c). Flow cytometry reveals that CD82 KO FRCs lack surface expression of both endogenous and CFP-tagged podoplanin (Fig. 2c i), but transfection efficiency and CFP expression is comparable (Fig. 2c ii). Since the CFP signal is derived from the PDPN-CFP fusion protein, we conclude that PDPN-CFP is expressed by CD82 KO cells, but that tetraspanin CD82 regulates podoplanin surface expression by controlling intracellular protein trafficking.

CD44 and CD9 control podoplanin membrane expression and balance hypercontractility. Two membrane binding partners of podoplanin have been identified: the hyaluronan receptor CD44 (33) and tetraspanin CD9 (40). We sought to investigate the role of podoplanin membrane binding partners CD44 and CD9 in modulating podoplanin expression and function. It has been shown that podoplanin-mediated hypercontractility can be counterbalanced by increased CD44 expression (24, 33), which requires podoplanin to localise to cholesterol-rich domains (24). Indeed, cholesterol depletion in FRCs results in increased contractility and cell rounding in a podoplanin-dependent manner (24). Tetraspanins are predicted to have an intramembrane cholesterol binding pocket controlling their activity (46). We hypothesise that podoplanin activity in FRCs is balanced through changing microdomains in the plasma membrane, stabilised by membrane binding partners CD44 and CD9.

To study the impact of CD44 and CD9 in podoplanin function in FRCs, we generated CD44 KO, CD9 KO and CD44/CD9 double knockout (DKO) polyclonal FRC lines using CRISPR/Cas9 editing (Fig. 3a). Deletion of either CD44 or CD9 in FRCs results in approximately 25% reduction of podoplanin surface expression compared to control FRCs (Fig. 3a), suggesting that the availability of these binding partners is a controlling factor in podoplanin expression levels at the plasma membrane. Interestingly, CLEC-2 binding to FRCs regulates *Cd44*, *Cd9*, and *Cd82* mRNA levels in addition to podoplanin (Supplementary Fig. 2, and Fig. 1). *Cd44* is upregulated in response to CLEC-2, in line with

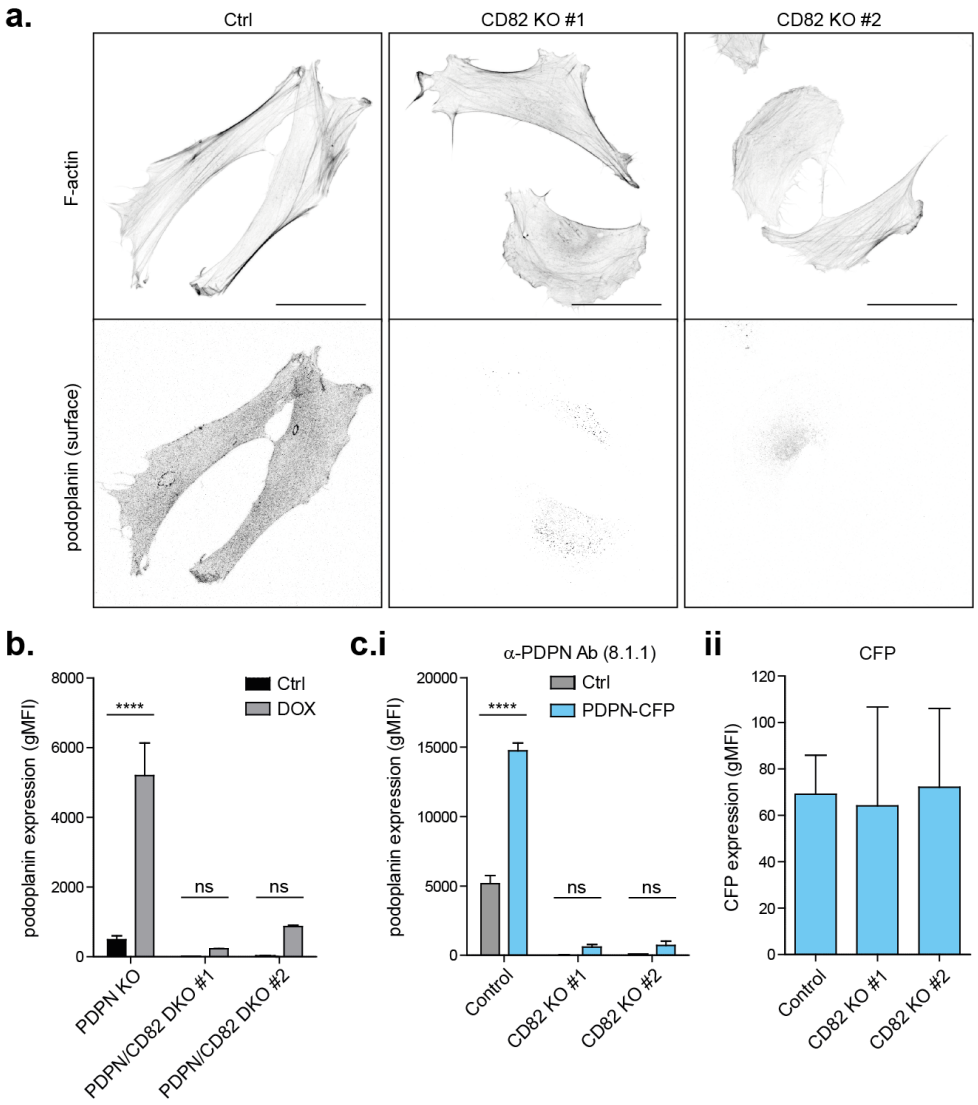

Fig. 2. Tetraspanin CD82 regulates podoplanin expression and localisation. **a.** Immunofluorescence of podoplanin surface expression (bottom row) on control (Ctrl) and two CD82 knock-out (KO) FRC cell lines. F-actin staining is used to visualise individual FRCs (top row). Maximum Z stack projections of representative images are shown. The scale bars represent 50 microns. **b.** Podoplanin KO (PDPN KO) and podoplanin/CD82 double-KO (PDPN/CD82 DKO) FRCs expressing a doxycycline-driven podoplanin-inducible plasmid were cultured in absence (black) or presence (grey) of doxycycline (DOX) for 48 hours. Podoplanin surface expression was analysed by antibody labelling using flow cytometry. **c.** Control and two CD82 KO FRC cell lines were transfected with CFP-tagged podoplanin (PDPN-CFP). Podoplanin surface expression using anti-mouse podoplanin antibody (clone 8.1.1; **i**) or CFP (**ii**) expression was analysed by flow cytometry. b-c. Data shown as mean+SD, n=3. ****p<0.0001, Two-way ANOVA with Tukey's multiple comparisons. ns, not significant. gMFI, geometric mean fluorescence intensity.

Pdpn mRNA (Supplementary Fig. 2b). Furthermore, CD44 surface protein levels are >30% lower in podoplanin shRNA knock-down (PDPN KD) FRCs, suggesting that podoplanin and CD44 are co-regulated transcriptionally and require one another for stable membrane expression (Supplementary Fig. 2b). However, *Cd82* and *Cd9* mRNA are both downregulated by CLEC-2 stimulation (Supplementary Fig. 2a,c). Similarly to CD44, CD9 surface expression is reduced by >50% in PDPN KD FRCs (Supplementary Fig. 2c). These data indicate there is co-regulation and a co-dependence in expression of podoplanin and its binding partners CD44 and CD9.

Since the predominant phenotype of podoplanin overexpression is high actomyosin contractility (24), we examined the role of CD44 and CD9 in controlling endogenous podoplanin-mediated actomyosin contractility in FRCs. FRCs remain spread in the absence of either CD44 or CD9, however, simultaneous deletion of both CD44 and CD9 (CD44/CD9 DKO) markedly increases FRC contractility (Fig. 3b), despite podoplanin levels being lower than in control cells (Fig. 3a). CD44/CD9 DKO cells round up and exhibit membrane blebbing (approximately 40% of cells; Fig. 3b). These results suggest that both CD44 and CD9 inhibit podoplanin-driven contractility in a non-redundant manner. Interestingly, these data also indicate that in the absence of either binding partner, the other is able to compensate to control hypercontractility. As it is known that podoplanin can directly bind to CD44 and/or CD9 (33, 40), these data predict that distinct populations of podoplanin molecules exist on the surface of FRCs, which are either inactive or contribute to functions beyond actomyosin contractility.

Podoplanin ligand function is independent of CD44 or CD9. Prior to the discovery that podoplanin could control actomyosin contractility intrinsically (24, 25), it was known to function as a ligand for the C-type lectin-like receptor CLEC-2, inducing both platelet aggregation and dendritic cell migration (14, 47). We tested whether CD44 or CD9 expression by FRCs is required for podoplanin ligand function using a three-dimensional co-culture of FRCs with bone marrow-derived dendritic cells, matured with lipopolysaccharide (LPS) to upregulate CLEC-2 expression (48). Binding to podoplanin$^+$ FRCs induces dendritic cells to ex-

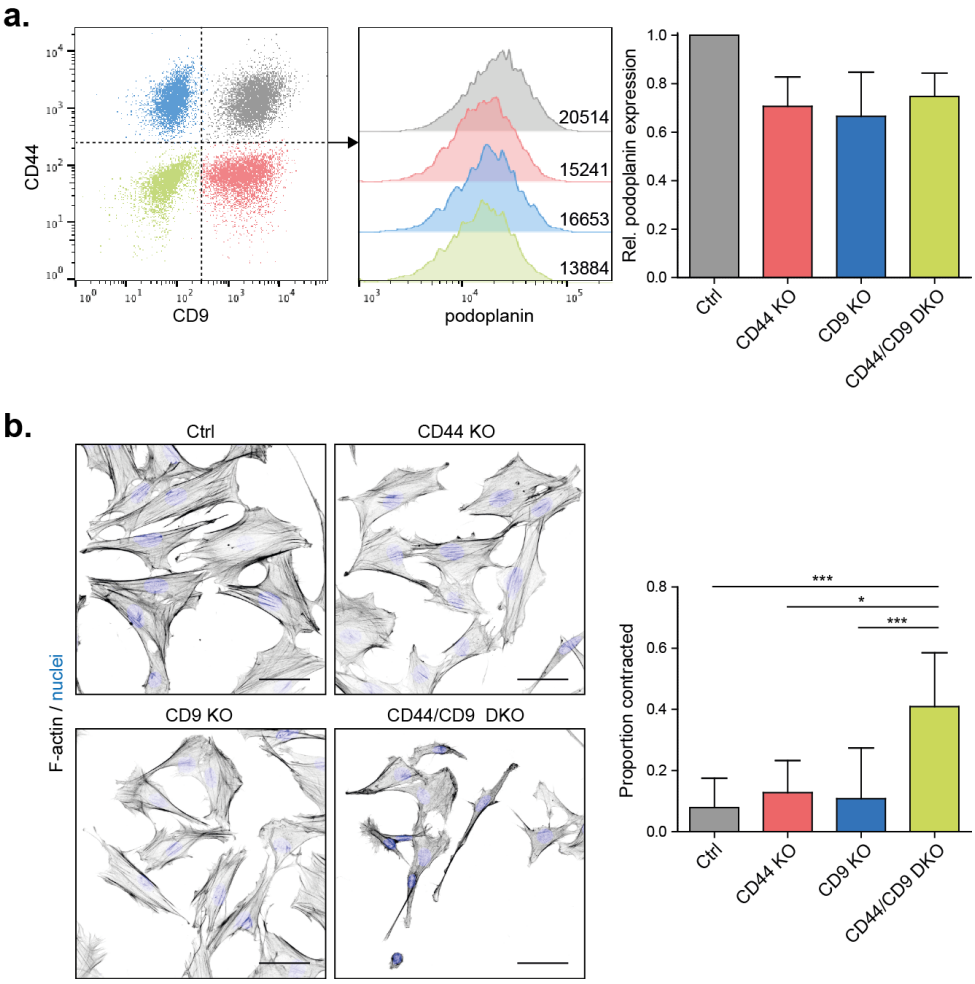

Fig. 3. CD44 and CD9 are required for stable podoplanin membrane expression and balancing hypercontractility. a. Analysis of podoplanin surface expression on control (Ctrl; grey), CD44 knock-out (KO; red), CD9 KO (blue), and CD44/CD9 double-KO (DKO; green) FRC cell lines by flow cytometry. Podoplanin expression is normalized to the level in Ctrl FRCs for each individual experiment. Data shown as mean+SD, n=3. **b.** Left: Immunofluorescence of F-actin (black) and cell nuclei (blue) in Ctrl, CD44 KO, CD9 KO, and CD44/CD9 DKO FRC cell lines. Maximum Z stack projections of representative images are shown. The scale bars represent 50 microns. Right: Proportion of contracted FRCs analysed in 13-15 images per cell line from 3 independent experiments. Data shown as mean+SD. *p<0.05, ***p<0.001, Kruskal-Wallis test with Dunn's multiple comparisons.

tend protrusions, in a CLEC-2 (47) and tetraspanin CD37-dependent manner (49). Whereas dendritic cells co-cultured with PDPN KD FRCs do not spread or make protrusions, co-culture of dendritic cells with CD44 KO or CD9 KO FRCs does not hamper dendritic cell responses (Fig. 4a), and the increase in morphology index is equivalent to dendritic cells co-cultured with control FRCs (Fig. 4b). Thus, podoplanin ligand function is not dependent on CD44 or CD9 expression on FRCs. This is in agreement with published data showing that soluble recombinant podoplanin-Fc can induce dendritic cell protrusions (47, 49).

CD44 and CD9 control FRC spreading in response to CLEC-2$^+$ dendritic cells. Since neither CD44 or CD9 are required for podoplanin-driven actomyosin contractility, or podoplanin ligand function, we next asked the reciprocal question: whether CD44 and/or CD9 are required for FRCs to respond to CLEC-2. Binding of CLEC-2^{hi} dendritic cells to FRCs drives elongation and spreading, which *in vivo*, is required for acute lymph node expansion during adaptive immune responses (24, 25). Dendritic cell contact results in control FRC spreading, defined by the reduction of F-actin filaments and the formation of multiple lamellipodia-like protrusions (Fig. 5a). This is quantified by increased morphology index (Fig. 5b), which is predominantly driven by an increase in perimeter rather than cell area (data not shown). Strikingly, CD44 KO and CD9 KO FRCs are unable to spread in response to dendritic cells (Fig. 5a-b) and both cell lines exhibit defective protrusion formation (Fig. 5a). CD44 KO FRCs exhibit small protrusions with F-actin 'spikes', whereas CD9 KO FRCs attempt broad, rounded protrusions, but fail to accumulate F-actin at the leading edge (Fig. 5a). CD44/CD9 DKO FRCs show a complete failure to make any protrusion in response to dendritic cell contact (Fig. 5c). These data indicate that both CD44 and CD9 participate in FRC spreading via parallel, non-redundant mechanisms.

FRCs require CD44 and CD9 to control podoplanin-driven contractility in steady-state (Fig. 3b), but not to bind to CLEC-2 (Fig. 4). Interestingly, we notice that although CD44/CD9 DKO FRCs do not make protrusions in response to CLEC-2$^+$ dendritic cells, there is still a clear reduction in F-actin (Fig. 5c). This indicates that CLEC-2$^+$ dendritic cells are still binding to podoplanin in the absence of CD44 and CD9, and that this engagement is sufficient to uncouple podoplanin from driving actomyosin contractility. Indeed, dendritic cell binding completely rescues the hypercontractile phenotype of CD44/CD9 DKO FRCs, which now remain spread (Fig. 5c). These data lead us to conclude that the induction of spreading and formation of protrusions in response to dendritic cell contact is an active process, and not a

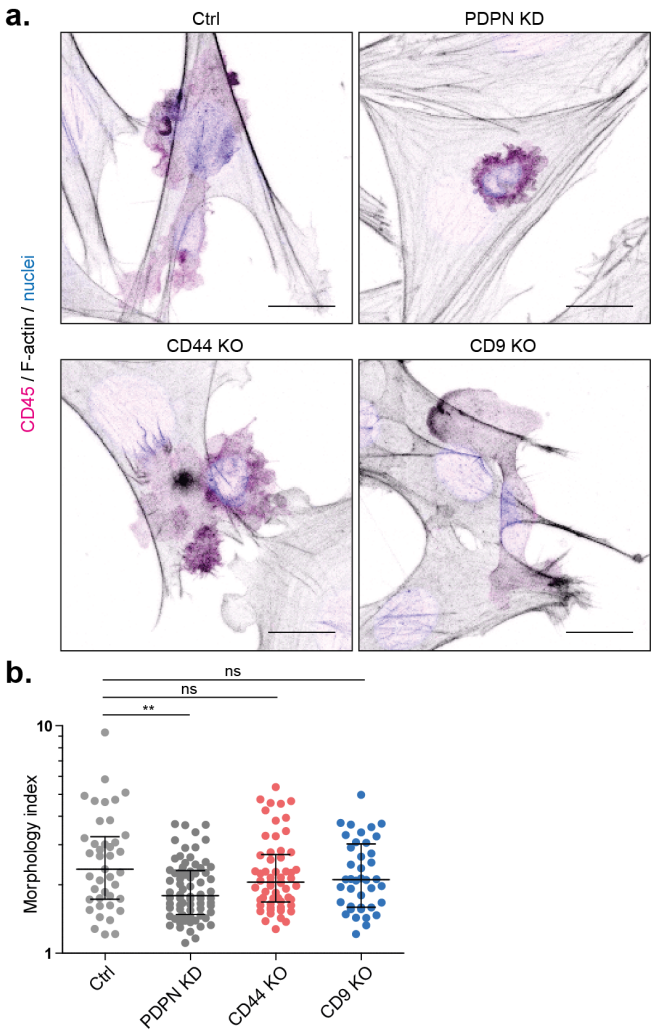

Fig. 4. Podoplanin ligand function is independent of CD44 or CD9. a. Immunofluorescence of three dimensional cultures of control (Ctrl), podoplanin siRNA knock-down (PDPN KD), CD44 knock-out (KO) or CD9 KO FRCs plus LPS-stimulated bone marrow-derived dendritic cells (CD45$^+$; magenta). Maximum Z stack projections of representative images are shown. The scale bars represent 20 microns. **b.** Morphology index (=perimeter^2/4πarea) of dendritic cells in interaction with an FRC. Dots represent single dendritic cells. Error bars represent median with interquartile range. $^{**}p<0.01$, Kruskal-Wallis test with Dunn's multiple comparisons. ns, not significant. Y-axis, log 10 scale.

downstream, indirect consequence linked to the loss of contractility (Fig. 5d). Furthermore, that the active induction of FRC spreading and formation of protrusions requires both podoplanin/CD44 and podoplanin/CD9 complexes.

CD44 and CD9 control distinct membrane pools of podoplanin. Since CD44 KO and CD9 KO FRCs both fail to form protrusions in response to dendritic cells, but exhibit quite different phenotypes (Fig. 5a-b), we sought to determine the differential roles of CD44 and CD9 in controlling podoplanin function and FRC morphology in the steady state. CLEC-2 binding to podoplanin results in loss of RhoA activity and an increase in Rac1 activity (24). Rac1 nucleates Arp2/3, which drives formation of new actin filaments, branching from pre-existing filaments in the cortical actin network, at the leading edge of lamellipodia (50). We examined Arp2/3$^+$ protrusions in CD44 KO and CD9 KO FRCs. Both CD44 KO and CD9 KO FRCs show increased membrane Arp2/3$^+$ localisation in cell protrusions compared to control FRCs (Fig. 6a), but the morphology and F-actin organisation within those protrusions is quite different. CD44 KO FRCs exhibit small Arp2/3$^+$ protrusions, and protrusions from different cells appear to meet and interact with each other (Fig. 6a). In contrast, CD9 KO FRCs have broad Arp2/3$^+$ protrusions, covering most of the plasma membrane, and the FRCs overlap each other (Fig. 6a).

To gain more insight, we investigated the membrane localisation of both proteins on FRCs. CD44 is expressed over the whole cell membrane, but is strongly enriched at the cell periphery where CD44 co-localises with podoplanin (Fig. 6b). In contrast, CD9 is present in punctate structures along the cell periphery and enriched in filopodia-like protrusions, where it partially co-localises with podoplanin (Fig. 6c). Neighbouring FRCs use filopodia-like protrusions to interact, and CD9 expression is enriched at the tips of these protrusions (Fig. 6c). Together, these data suggest that CD44 and CD9 are involved in two different modes of protrusion formation. Furthermore, podoplanin co-localises with CD44 and CD9 in both types of protrusions, supporting the idea that there are distinct pools of podoplanin on the FRC cell membrane. We cannot rule out presence of CD82 in these distinct podoplanin pools, as we were unable to visualize localisation of CD82 protein on FRCs due to lack of an appropriate antibody.

Previous findings show that upon CLEC-2 stimulation, podoplanin co-localises in cholesterol-rich domains (24), which also contain CD44 (41). However, there were also podoplanin protein clusters excluded from cholesterol-rich domains (24), and our data now suggests that these clusters may contain CD9. Furthermore, our data suggests that CD9 is required for sensing neighbouring cells and establishing interactions, in agreement with other studies showing roles for CD9 in cell fusion (51) and adhesion (52). CD9 expression by FRCs may therefore contribute to FRC network formation *in vivo*.

Podoplanin, CD44 and CD9 are co-regulated *in vivo* during lymph node expansion. FRC spreading is a piv-

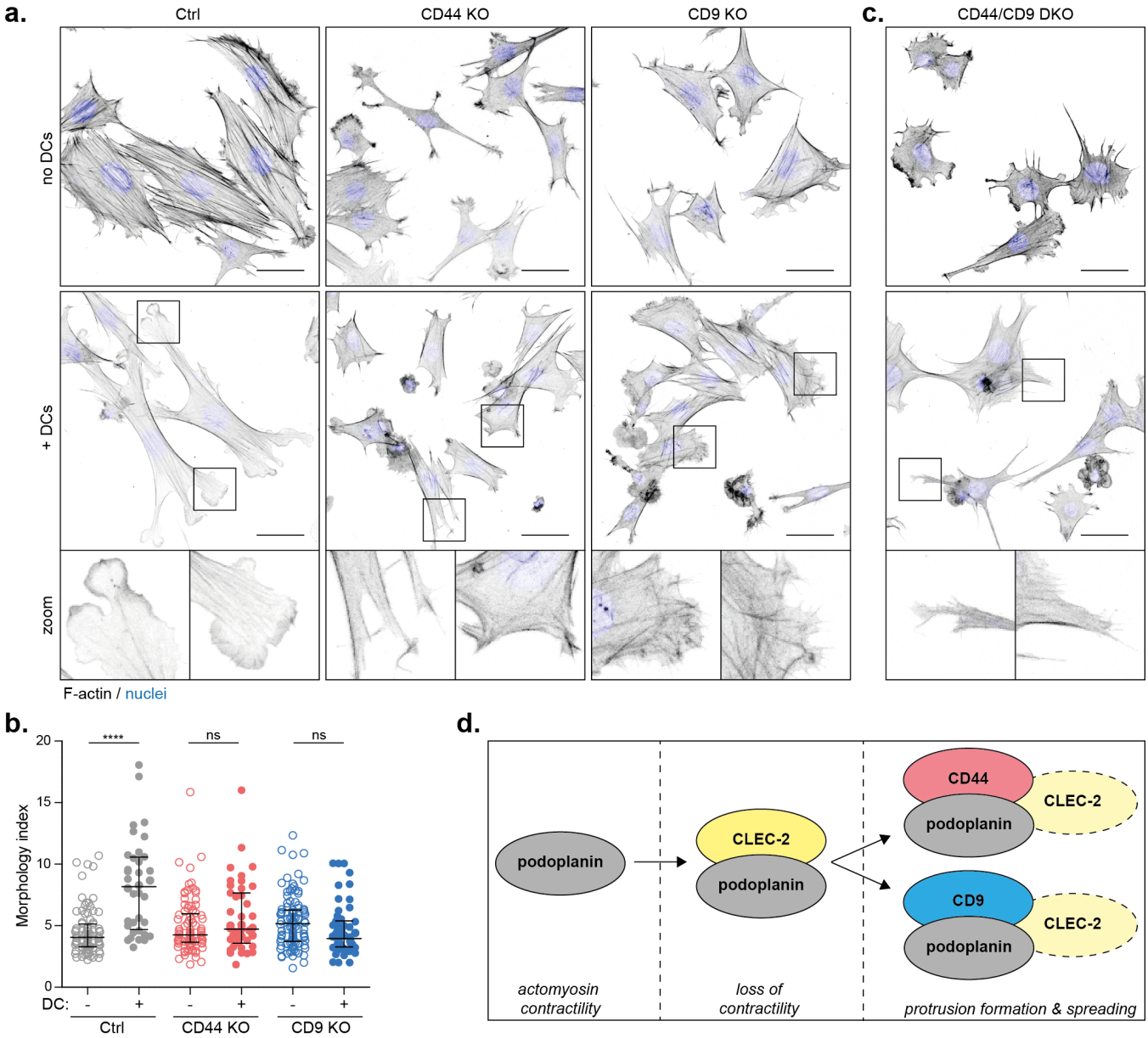

Fig. 5. CD44 and CD9 are both required for FRC spreading in response to CLEC-2⁺ dendritic cells. a-c. Immunofluorescence of three-dimensional cultures of control (Ctrl), CD44 knock-out (KO), CD9 KO (**a**), or CD44/CD9 double-KO (DKO; **c**) FRCs without (upper row) or with (middle and bottom rows) LPS-stimulated bone marrow-derived dendritic cells (DC). Maximum Z stack projections of representative images are shown. The scale bars represent 50 microns. Morphology index (=perimeter^2/4πarea; **b.**) of control (Ctrl, grey), CD44 KO (red) and CD9 KO (blue) FRCs in interaction with a dendritic cell. Dots represent single FRCs. Error bars represent median with interquartile range. ****p<0.0001, Two-way ANOVA with Tukey's multiple comparisons. ns, not significant. **d.** Schematic representation of the function of podoplanin (grey) without and with its binding partners CLEC-2 (yellow), CD44 (red) and CD9 (blue).

otal step in initiation of lymph node expansion (24, 25). This is induced by migratory CLEC-2^{hi} dendritic cells entering the lymph node. These dendritic cells migrate to the lymph node via the efferent lymphatic vessels, before migrating through the subcapsular sinus to reach the paracortex. The lymph node is a highly structured organ consisting of different functional zones, which are organised and defined by different FRC subsets (53, 54). CLEC-2^{hi} migratory dendritic cells will first come in contact with marginal reticular cells (MRCs), a subset of FRCs defined by expression of MAdCAM-1 and located below the subcapsular sinus and in the interfollicular regions (55). MRCs play an important role in lymph node development, antigen transport to the B-cell follicles, plasma B-cell homeostasis and provide a niche for subcapsular sinus macrophages (55–60). Furthermore, MRCs are suggested to play a role in dendritic cell transmigration from the subcapsular sinus to the T-cell zone (61). In the T-cell zone, CLEC-2^{hi} migratory dendritic cells will interact with podoplanin-expressing T-zone FRCs (TRCs) resulting in TRC elongation and spreading.

In order to investigate the role of CD44 and CD9 in FRC spreading *in vivo*, we immunized mice with IFA/OVA. Despite a rapid increase in lymph node size (data not shown) and cellularity (Fig. 7a), FRC numbers do not significantly increase in the first week post-immunization (Fig. 7b), indicative of the acute spreading phase of lymph node expan-

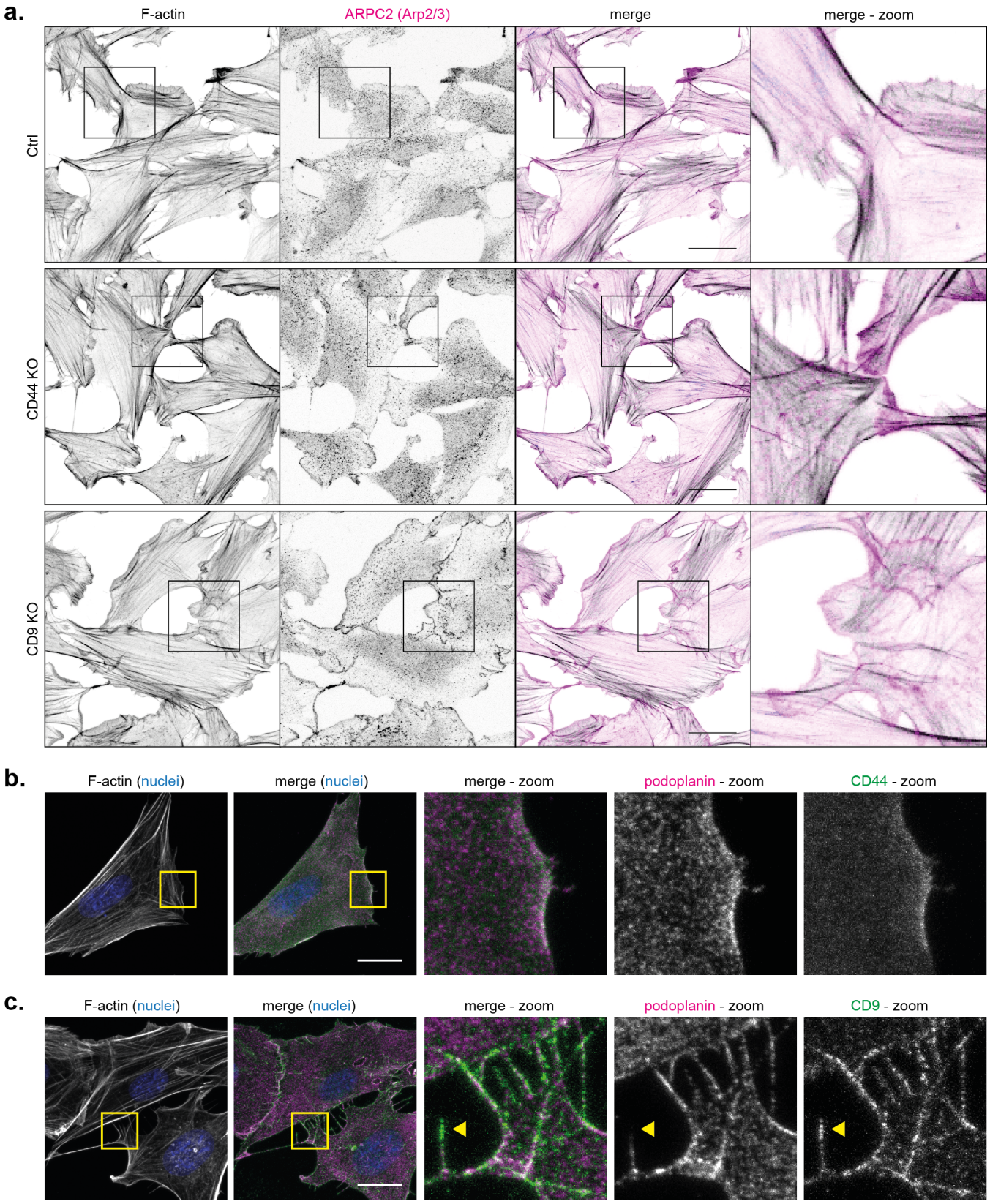

Fig. 6. CD44 and CD9 control distinct domains of podoplanin. a. Immunofluorescence of Arp2/3^{+} protrusions (magenta) in control (Ctrl, upper row), CD44 knock-out (KO; second row) and CD9 KO (bottom row) FRCs. Maximum Z stack projections of representative images are shown. The scale bars represent 30 microns. **b-c.** Immunofluorescence of podoplanin (magenta) and CD44 (**b**; green) or CD9 (**c**; green) in control FRCs. Maximum Z stack projections of representative images are shown. The scale bars represent 20 microns. Yellow arrow head indicates filopodia tip.

sion (24). Within these first 5 days, podoplanin expression is upregulated on both TRCs (PDPN$^+$CD31$^-$MAdCAM-1$^-$; Fig. 7c) and MRCs (PDPN$^+$CD31$^-$MAdCAM-1$^+$; Fig. 7d). Interestingly, podoplanin expression decreases and returns to baseline levels as FRCs begin to increase in number (Fig. 7b-d). Next, we determined CD44 and CD9 expression levels on TRCs and MRCs (Fig. 7c-d). On TRCs, both CD44 and CD9 expression are upregulated in parallel with podoplanin expression (Fig. 7c), providing further evidence for their role in binding to podoplanin and regulating TRC spreading. In contrast, MRCs do not alter their expression of CD44 and CD9 (Fig. 7d). MRCs are located in the periphery of the lymph node and will experience different mechanical forces to the TRC network, which stretches and expands to accommodate proliferating T cells (18, 24, 25). These data indicate that the increased expression of CD44 and CD9 is required specifically by TRCs, and adds to our understanding that FRCs in different lymph node microenvironments have different phenotypes and functions.

Taken together, our data demonstrate that podoplanin function on FRCs is regulated by the balance of interactions with its membrane binding partners. By this mechanism, podoplanin function can be switched to control both actomyosin contractility, and cell spreading and protrusion formation. *In vivo*, these key podoplanin binding partners, CD44 and CD9, are upregulated during the acute stretching phase of lymph node expansion to contribute to initiation of an adaptive immune response.

Discussion

FRC spreading is a pivotal first step of the immune response allowing lymph node expansion to accommodate proliferating T lymphocytes (24, 25). Our results now show that FRCs require podoplanin binding partners CD44 and CD9 to form cell protrusions and to spread in response to CLEC-2^{hi} dendritic cells. *In vivo*, we find that CD44 and CD9 levels simultaneously increased with podoplanin levels on TRCs in the first 3-5 days post-immunization. Interestingly, although CD44 and CD9 levels do not increase on MRCs, as do podoplanin levels, baseline levels of CD44 and CD9 are approximately 2-fold higher compared to TRCs. MRCs are located beneath the subcapsular sinus and are in close contact with resident macrophages, suggesting they play a role in immune homeostasis (61, 62). As such, MRCs have frequent interactions with antigen-activated immune cells, like macrophages and dendritic cells, which can both express CLEC-2 (49). We therefore hypothesize that MRCs constantly encounter CLEC-2$^+$ cells, perhaps explaining the higher baseline levels of podoplanin, CD44 and CD9. In contrast, TRCs will only respond upon an influx of CLEC-2$^+$ dendritic cells into the T-cell zone during an adaptive immune response. In line with this, *Cd44* has been identified as a differently expressed gene on *Cxcl9*$^+$ TRCs, an activated TRC subset present in the T-cell zone and interfollicular regions (54). Our data adds to our understanding of the different niches within the lymph node, and the role of these local microenvironments in controlling cell phenotypes.

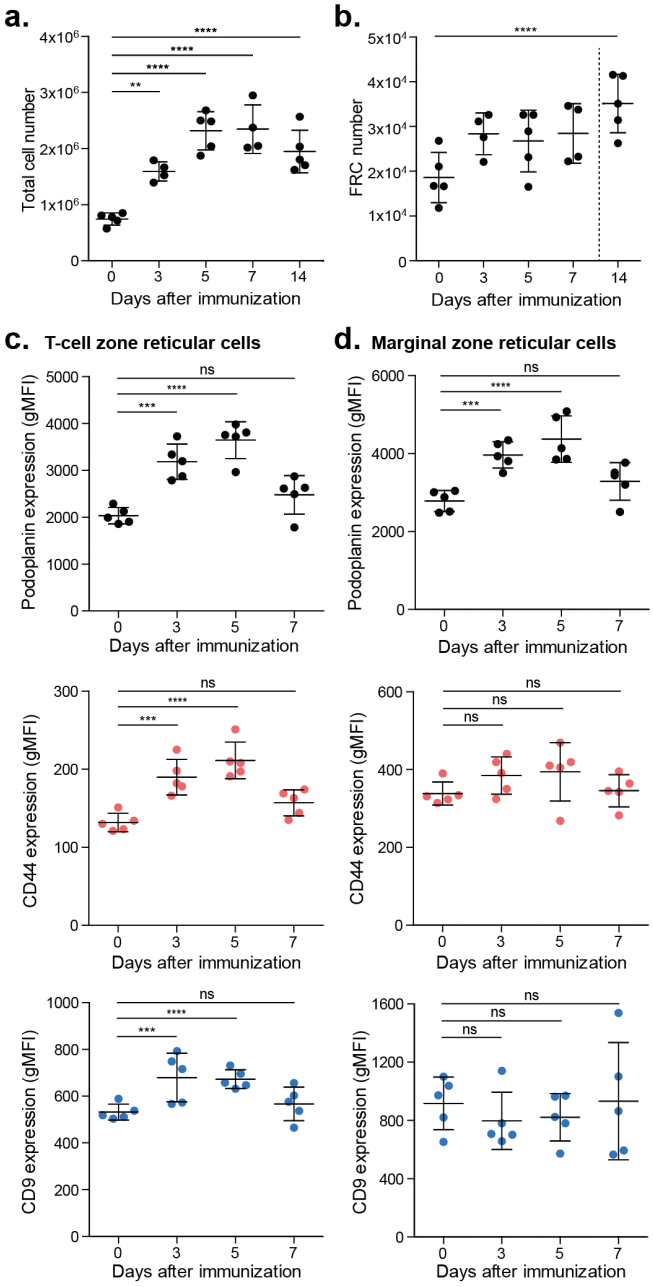

Fig. 7. Podoplanin, CD44 and CD9 expression on FRCs increases upon in vivo immunisation. Analysis by flow cytometry of cell suspensions of inguinal lymph nodes from C57BL/6 mice immunized with IFA/OVA for indicated time points. **a.** Total live cell number based on counting beads and live-dead staining as measured by flow cytometry. **b.** FRC number. Dashed line separates FRC spreading (left) from FRC proliferation (right) phase. **c-d.** Podoplanin (top), CD44 (middle) and CD9 (bottom) surface expression on T-zone reticular cells (TRC; podoplanin$^+$CD31$^-$MAdCAM-1$^-$; **c**) or on marginal reticular cells (MRC; podoplanin$^+$CD31$^-$MAdCAM-1$^+$; **d**). **a-d.** n=4-5 mice per time point. FRC population was based on total lymph node cell count x (percentage of live cells) x (percentage of CD45$^-$ cells). *p<0.05, **p<0.01, ****p<0.0001, One-way ANOVA with Tukey's multiple comparisons. ns, not significant. gMFI, geometric mean fluorescence intensity.

Podoplanin is intimately connected with cytoskeletal regulation, contractility and protrusion formation, yet in FRCs neither of these processes is coupled to cell migration (1, 17). It had been assumed that FRC spreading was an indirect event in response to loss of actomyosin contractility (24, 25), but we now identify loss of actomyosin contractility and spreading as two differently regulated, but linked processes. In the lymph node, FRCs form an intricate network in which the cells function together as a population and not as individual cells (63, 64). During an immune response, proliferating T cells provide a mechanical strain for TRCs (18), and cell spreading is required to preserve network connectivity throughout lymph node remodelling in which cells stay in position relative to their neighbours. Since we recently identified that FRCs exhibit a type of apical to basolateral polarity, in order to secrete matrix components unilaterally into conduit structures (43), this may explain the lack of front to back polarity which would be required for cell migration. Although CD9 is important in other cell types for migration (65), our data indicate that in FRCs, CD9 is involved in cell-cell connections, thereby contributing to the formation and preservation of the FRC network.

Overexpression of podoplanin can drive hypercontractility (24), but we determine that normal expression of CD44 or CD9, or binding to CLEC-2^{+} DCs is able to counterbalance podoplanin-driven contractility. Subsequently, CD44/podoplanin and CD9/podoplanin complexes can both promote protrusion formation in presence of CLEC-2, but CLEC-2 stimulation cannot induce FRC spreading in the absence of either CD44 or CD9. Actomyosin contractility in FRCs depends on ERM binding to the intracellular tail of podoplanin (24, 25). CLEC-2 binding inhibits actomyosin contractility, and drives podoplanin localisation to cholesterol-enriched domains (24). CD44 is also known to reside in cholesterol-enriched domains (41), and to bind ERM proteins (66). It has recently been suggested that not the ectodomain of podoplanin (33), but its transmembrane or cytoplasmic domains are required to bind CD44 (1). This, together with our data, supports the hypothesis that CLEC-2 binding drives the localisation and interaction of podoplanin and CD44 in cholesterol-rich domains, and that this binding prevents both podoplanin and CD44 from binding to ERM proteins with their cytoplasmic domains. It is currently unknown if CLEC-2-mediated clustering of podoplanin and CD44 forces uncoupling of ERM proteins, or if dephosphorylation and uncoupling of ERM proteins by an unknown mechanism provides space for clustering of podoplanin and CD44. Further studies are required to identify the specific order of signalling events downstream the CLEC-2/podoplanin axis. Our data suggest that the function of podoplanin would be determined not by expression level or subcellular localisation, but by the balance of membrane binding partners; and that it is these binding partners CD44 and CD9 that control the balance of podoplanin activity, between actomyosin contractility and protrusion formation.

We have examined podoplanin function in FRCs which exhibit high endogenous expression in homeostasis (7). Podoplanin expression can also be induced in various pathologies, such as cancer and wound healing (1, 17). We now identify that one mechanism to upregulate podoplanin expression is the binding of CLEC-2, which results in a transcriptional increase of *Pdpn*. Tumour cells and CAFs often reside in microenvironments of poorly structured vasculature and leaking vessels (67). CLEC-2^{hi} platelets may potentially bind tumour cells and CAFs to upregulate podoplanin expression, influencing tumour progression.

Furthermore, we find that CD82 is required for podoplanin expression in FRCs; a more dramatic phenotype than reported in CD82 KO osteoclasts which showed reduced podoplanin expression (45). Our data suggests that CD82 controls podoplanin trafficking to the plasma membrane, which is a well-known function of tetraspanin family members (44). This hypothesis is supported by induced co-expression of podoplanin (8) and CD82 (68) in rheumatoid arthritis-associated synovial fibroblasts. It is unknown if CD82 is a direct partner of podoplanin, or indirectly binds to podoplanin via another, potentially unknown, binding partner. We suggest that podoplanin activity in other cellular systems would also depend on the expression of CD82, or may be trafficked to the cell surface by alternative tetraspanins in different cellular contexts.

Together, this study provides molecular understanding of how podoplanin as one protein drives multiple functions in different cellular contexts. Podoplanin interactions with different binding partners provide a molecular switch for cells to respond to changing microenvironments.

Materials and methods

Mice. Wild-type C57BL/6J mice were purchased from Charles River Laboratories. PDGFRαKI$^{H2B\text{-}GFP}$ mice (B6.129S4-Pdgfrαtm11(EGFP)Sor/J) were purchased from Jackson Laboratories and used for preferential localization of PDGFRα^{+} FRCs by fluorescence labelling of cell nuclei (GFP^{+}). Both males and females were used for *in vivo* and *in vitro* experiments and were aged 6–10 weeks. All mice were age matched and housed in specific pathogen-free conditions. All animal experiments were reviewed and approved by the Animal and Ethical Review Board (AWERB) within University College London and approved by the UK Home Office in accordance with the Animals (Scientific Procedures) Act 1986 and the ARRIVE guidelines.

***In vivo* immunizations.** Mice were immunized via subcutaneous injection in the right flank with 100 μl of an emulsion of OVA in complete (CFA) or incomplete (IFA) Freund's adjuvant (100 μg OVA per mouse; Hooke Laboratories). Inguinal lymph nodes from both flanks (draining and non-draining) were taken for analysis by flow cytometry or immunofluorescence. Lymph nodes were digested as previously described (Fletcher et al., 2011), and cells were counted using Precision Count Beads as per supplier's instructions (Biolegend), and stained for analysis by flow cytometry.

Cell lines and primary cell culture. Control and podoplanin knockdown (PDPN KD) FRC cell lines (Acton et al., 2014), and CLEC-2-Fc expressing FRCs (Martinez et al., 2019) are previously described. Podoplanin knock-out (PDPN KO) FRC cell line was generated using CRISPR/Cas9 editing. Control FRC cell line (Acton et al., 2014) was transfected with pRP[CRISPR]-hCas9-U6>PDPN gRNA 1 plasmid (constructed and packaged by Vectorbuilder; vector ID: VB160517-1061kpr) using Lipofectamine 2000 Transfection Reagent (Thermo Fisher Scientific). We performed three rounds of transfection, and subsequently performed magnetic cell sorting (MACS) using MACS LD columns (Miltenyi Biotec), anti-mouse podoplanin-biotin antibody (clone 8.1.1, eBioscience, 13-5381-82), and anti-biotin microbeads (Miltenyi Biotec, 130-090-485) as per supplier's instructions to sort PDPN KO FRCs by negative selection. Complete knockout of podoplanin expression was confirmed using RT-PCR, flow cytometry and Western blot.

Doxycycline-inducible podoplanin-expressing FRCs were generated using the piggyBac transposon-based expression system (Li et al., 2013). PDPN KO FRCs were transfected using Attractene Transfection Reagent (Qiagen) with the following three plasmids at a ratio of 1:1:1 - 1) plasmid carries the EF1A promotor, to drive the expression of Tet3g, and a puromycin resistance gene (constructed and packaged by Vectorbuilder; vector ID: VB151009-10079), 2) doxycycline-inducible plasmid carrying TRE3G, which drives the expression of murine podoplanin together with the fluorescence marker Cypet tagged to P2A which allows self-cleavage from podoplanin upon translation and a blasticidin resistance gene with mCherry for selection after transfection (constructed and packaged by Vectorbuilder; vector ID: VB151008-10006), and 3) plasmid expressing PBase (Li et al., 2013). Transfected cells were selected with puromycin and blasticidin (both Invivogen). Cells were treated with 1 μg/ml doxycycline for 48 hours followed by MACS and flow associated cell sorting (FACS) to select for podoplanin expressing cells.

CD44 KO, CD9 KO, CD44/CD9 DKO, and CD82 KO FRCs were generated using CRISPR/Cas9 editing. Control or (podoplanin-inducible) PDPN KO FRCs were transfected using Attractene Transfection Reagent (Qiagen) with one or both of the following plasmids: pRP[CRISPR]-hCas9-U6>CD44-T3 exon 2 (constructed and packaged by Vectorbuilder; vector ID: VB180119-1369pus), pRP[CRISPR]-hCas9-U6>CD9 exon 1 (constructed and packaged by Vectorbuilder; vector ID: VB180119-1305adb), or pRP[CRISPR]-hCas9-U6>CD82-T1 exon 5 (constructed and packaged by Vectorbuilder; vector ID: vector ID VB180119-1391uky). Subsequently, CD44 KO, CD9 KO, and CD44/CD9 DKO FRCs underwent two or three rounds of FACS to obtain a full CD44 and/or CD9 KO FRC cell line, which was confirmed using flow cytometry (Fig. 3a), RT-PCR, and Western blot (data not shown). For generation of CD82 KO FRCs, a GFP expressing plasmid was co-transfected, and 3 days after transfection, GFP^+ cells were selected using FACS, and cultured in 96-well plates (approx. 1 cell per well) to obtain single cell clones. Complete knockout of CD82 expression was confirmed using RT-PCR (Supplementary Fig. 1).

FRC cell lines were cultured in high-glucose DMEM with GlutaMAX supplement (Gibco, via Thermo Fisher Scientific) supplemented with 10% fetal bovine serum (FBS; Sigma-Aldrich), 1% penicillin-streptomycin (P/S) and 1% insulin-transferrin-selenium (both Gibco, via Thermo Fisher Scientific) at 37°C, 10% CO_2, and passaged using cell dissociation buffer (Gibco, via Thermo Fisher Scientific).

Primary cell isolation from murine lymph nodes was performed as previously described (Fletcher et al., 2011), cultured as described above, and treated with 20 μM ROCK inhibitor (Y-26732 dihydrochloride, Tocris, 1254) for indicated time points. Culture medium was changed every 3 days, upon which fresh Y-27632 was added.

Bone marrow-derived dendritic cells (BMDCs) were generated by culturing murine bone marrow cell suspensions in RPMI 1640 medium (Gibco, via Thermo Fisher Scientific) supplemented with 10% FBS, 1% P/S and 50 μM 2-mercaptoethanol (Gibco, via Thermo Fisher Scientific), and 20 ng/ml recombinant murine granulocyte-macrophage colony-stimulating factor (mGM-CSF, Peprotech, 315-03), as adapted from previously described protocols (Lutz et al., 1999), at 37°C, 5% CO_2. On day 6, BMDCs were additionally stimulated with 10 ng/ml lipopolysaccharides from *E.coli* (LPS; Sigma-Aldrich, L4391-1MG) for 24 hours.

PDPN-CFP transfection. FRCs were plated in a 6-well culture plate ($5x10^4$ cells per well) one day before transfection with PDPN-CFP (Acton et al., 2012) (ratio 1:2) using Attractene transfection reagent (Qiagen) as per supplier's instructions. After 48 hours, FRCs were harvested for analysis of surface podoplanin and total PDPN-CFP expression by flow cytometry.

DC-FRC co-cultures. FRCs (0.7×10^4 cells per well) were seeded on 24-well glass-bottomed cell culture plates (MatTek) at 37°C, 10% CO_2. After 24 hours, LPS-stimulated BMDCs (2.5×10^5 cells per well) were seeded into 3D collagen (type I, rat tail)/Matrigel matrix (both from Corning, via Thermo Fisher Scientific) supplemented with 10% minimum essential medium alpha medium (MEMalpha, Invitrogen, via Thermo Fisher Scientific) and 10% FCS (Greiner Bio-One) on top of the FRCs. Co-cultures were incubated overnight at 37°C, 10% CO_2. The next day, cultures were fixed with AntigenFix (DiaPath, via Solmedia) for 3 hours at room temperature (RT), followed by permeabilization and blocking with 2% bovine serum albumin (BSA; Sigma-Aldrich) and 0.2% Triton X-100 in phosphate-buffered saline (PBS) for 2 hours at RT. Subsequently, BMDCs were stained using rat anti-mouse CD45-AF647 (clone 30-F11, 1:250, Biolegend, 103123), and F-actin and cell nuclei were visualized using respectively phalloidin-TRITC (P1951-1MG) and 4,6-diamidino-2-phenylindole (DAPI; D9542-1MG; both 1:500 dilution, both from Sigma-Aldrich). Co-cultures were imaged on a Leica SP5 confocal microscope using HCX PL APO /1.25 40x oil lenses, and analysed using Fiji/ImageJ

software. Z stacks (0.5 μm/step) were projected with ImageJ Z Project (maximum projection). Morphology index (=perimeter^2/4πarea) was calculated using the area and perimeter of BMDCs or FRCs by manually drawing around the cell shape using F-actin staining.

Immunofluorescence. Inguinal murine lymph nodes were fixed in AntigenFix (DiaPath, via Solmedia) overnight at 4°C, and subsequently washed and incubated in 30% sucrose (w/v) (Sigma-Aldrich) in PBS overnight at 4°C. Samples were embedded in Tissue-Tek® O.C.T. Compound (Thomas Scientific), frozen using 2-methylbutane (GPR RECTAPUR) and cooled with liquid nitrogen. 20 μm sections were cut using Leica CM1850 cryostat. For immunostaining, tissue sections were blocked and permeabilized for 2 hours at RT in 10% normal goat serum (Sigma-Aldrich) and 0.3% Triton X-100 (Sigma-Aldrich) in PBS. Tissue sections were incubated with hamster anti-mouse podoplanin monoclonal antibody (clone 8.1.1, 1 μg/ml, Acris Antibodies, DM3501) diluted in 10% normal goat serum (Sigma-Aldrich), 0.01% Triton X-100 (Sigma-Aldrich) in PBS overnight at 4C. Three washing steps were used to remove unbound antibody, before incubation with appropriate Alexa Fluor-conjugated secondary antibody (1:500, Invitrogen, via Thermo Fisher Scientific) for 2 hours at RT. Sections were washed and mounted in Mowiol (Sigma-Aldrich). Samples were imaged on a Leica TCS SP8 STED 3X using HC PL APO CS2 /1.4 63x oil lenses.
FRCs were seeded on glass coverslips for 24 hours at 37°C, 10% CO_2. Cells were fixed in 3.6% formaldehyde (Sigma-Aldrich; diluted in PBS), and subsequently blocked in 2% BSA in PBS and stained for 1 hour at RT with the following primary mouse antibodies: rabbit anti-p34-Arc/ARPC2 (Arp2/3, 1:100, Merck, 07-227), hamster anti-podoplanin-eFluor660 (clone 8.1.1, 1:200, eBioscience, 50-5381-82), rat anti-CD44 (clone IM7, 1:200, BD Biosciences, 553131), or rat anti-CD9 (clone KMC8, 1:200, eBioscience, 14-0091-82). This was followed by incubation with appropriate Alexa Fluor-conjugated secondary antibodies (1:500, Invitrogen, via Thermo Fisher Scientific) for 1 hour at RT. F-actin and cell nuclei were visualized using respectively phalloidin-TRITC (P1951-1MG) and DAPI (D9542-1MG; both 1:500 dilution, both from Sigma-Aldrich) incubated for 15 minutes at RT, and coverslips were mounted in Mowiol (Sigma-Aldrich). Cells were imaged on a Leica SP5 confocal microscope using HCX PL APO /1.4 63x oil lenses, and analysed using Fiji/ImageJ software. Z stacks (0.5 μm/step) were projected with ImageJ Z Project (maximum projection). Proportion of contracted cells was quantified by analysing the number of contracted/blebbing cells (based on F-actin staining) compared to total number of cells per field of view.

Flow cytometry. Single-cell suspensions were incubated with FcR blocking reagent (Miltenyi Biotec) as per supplier's instructions, followed by 30 minutes staining on ice with the following primary mouse antibodies diluted in PBS supplemented with 0.5% BSA and 5mM EDTA: rat anti-CD45-AlexaFluor700 (clone 30-F11, 0.5 μL/test, Biolegend, 103128), rat anti-CD31-AlexaFluor647 (clone MEC13.3, 0.5 μL/test, Biolegend, 102516), rat anti-CD140α-PE-Cy7 (clone APA5, 0.6 μL/test, eBioscience, 25-1401-80), hamster anti-podoplanin- AlexaFluor488 (clone 8.1.1, 1 μL/test, eBioscience, 53-5381-82), hamster anti-podoplanin-eFluor660 (clone 8.1.1, 1:200, eBioscience, 50-5381-82), rat anti-CD44-PE (clone IM7, 1:50, BD Biosciences, 553134), and/or rat anti-CD9-FITC (clone MZ3, 1:50, Biolegend, 124808). Stained cells were analyzed using LSR II or LSR-Fortessa X-20 flow cytometers (both BD Biosciences).
For analysis of lymph nodes from *in vivo* immunisations by flow cytometry, 3x10^6 cells were incubated with purified rat IgG2b anti-mouse CD16/32 receptor antibody as per supplier's instructions (Mouse BD Fc-block, clone 2.4G2, BD Biosciences, 553141) for 20 minutes at 4C. Cells were stained with the following primary mouse antibodies (1:100 dilution) for 30 minutes at 4C: CD45-BV750 (clone 30-F11, Biolegend, 103157), CD31-PE-Cy5.5 (clone MEC 13.3, BD Biosciences, 562861), podoplanin-PE (clone 8.1.1, BD Biosciences, 566390), CD44-BV605 (clone IM7, BD Biosciences, 563058), CD9-FITC (clone MZ3, Biolegend, 124808) and MAdCAM-1-BV421 (clone MECA-367, BD Biosciences, 742812). Cells were washed with PBS and stained with Zombie Aqua fixable live-dead kit as per supplier's instructions (Biolegend, 423101) for 30 minutes at 4C. Samples were analysed on BD Symphony A5 equipped with 355 nm, 405 nm, 488 nm, 561 nm and 638 nm lasers. Acquisition was set to 5x10^5 single, live CD45$^+$ cells. FRC cell number was based on their percentage within the CD45$^-$ cells. All flow cytometry data was analysed using FlowJo Software version 10 (BD Biosciences).

Western blot. Ctrl or CLEC-2-Fc FRCs were plated in a 6-well culture plate (1x10^5 cells per well). After 24 hours, the culture plate was placed on ice and cells were washed twice with cold PBS. Cells were lysed in 100 μl 4x Laemmli lysis buffer (Bio-Rad) and collected using cell scraper. Samples were separated by reducing 10% SDS-polyacrylamide gel electrophoresis. Western blots were incubated with rat anti-mouse podoplanin (clone 8F11, 1:1000, Acris Antibodies, AM26513AF-N), or mouse anti-Histone H3 (1:2000, Abcam, ab24824) as loading control, in PBS supplemented with 1% skim milk powder and 0.2% BSA overnight at 4°C, followed by staining with appropriate HRP-conjugated secondary antibodies (Abcam) for 2 hours at RT. Western blots were developed using Luminata Crescendo Western HRP substrate (Merck Millipore) and imaged on ImageQuant LAS 4000 mini (GE Healthcare Life Sciences).

Transcriptome sequencing and analysis. FRCs were cultured for 24 hours, adding 50 μg/ml CLEC-2-Fc from the beginning or 6 hours before collecting cells. Control FRCs were left untreated. RNA extractions were performed using RNAeasy Kit (Qiagen) as per supplier's instructions, including a DNA digestion step to avoid genome contamination. For transcriptome sequencing and analysis, RNA preparations from FRCs were sequenced to a depth of 9 million to 22 million reads by Queen Mary University (QMUL) Genome Centre. The raw read quality control was performed by the

QMUL Genome Centre using Basespace software (Illumina). Paired end FASTQ files were then aligned to Mus musculus GRCm38 reference assembly using STAR aligner software (Dobin et al., 2013). Transcripts were assembled and relative transcript abundance were calculated using Salmon software(Patro et al., 2017). Using R software (v3.4.4) and the Bioconductor tximport package (Soneson et al., 2016), transcripts per million (TPM) values were generated and annotated with ENSEMBL gene IDs. Bulk TPM data were categorised by fold change (>2 fold) between control, 6 hours and 24 hours conditions using an in-house developed R script.

RNA isolation and quantitative RT-PCR analysis. RNA lysates of Ctrl and CD82 KO FRCs were stored at -80°C until RNA isolation using RNeasy Mini kit (Qiagen) as per supplier's instructions, including a DNA digestion step to avoid genome contamination. RNA quantity and purity were determined on a NanoDrop spectrophotometer, and reverse transcribed to cDNA using SuperScript® IV First-Strand Synthesis System kit (Invitrogen, via Thermo Fisher Scientific) as per supplier's instructions. mRNA levels of *Pdpn* (transcript variant 1) or *Cd82* were determined with a CFX96 Sequence Detection System (Bio-Rad) with MESA Blue (Eurogentec, via Promega) as the fluorophore and gene-specific oligonucleotide primers. The following primers were used: *Pdpn* forward 5-CAGGGAGGGACTATAGGCGT, *Pdpn* reverse 5-TGTCTGCGTTTCATCCCCTG, *Cd82* forward 5-TGGACATCATTCGCAACTACAC, *Cd82* reverse 5-GCATGGGTAAGTGGTCTTGGTA. Reaction mixtures and program conditions were applied as recommended by the manufacturer (Bio-Rad). Quantitative RT-PCR data were analyzed with the CFX Manager software (version 3.1, Bio-Rad) and checked for correct amplification and dissociation of the products. Ct values of the genes of interest were normalized to the Ct value of the housekeeping gene *Gapdh*.

Statistics. Statistical differences between two groups were determined using unpaired Student's t-test. Statistical differences between more than two groups were determined using two-way ANOVA with Tukey's multiple comparisons test, or, in the case of non-Gaussian distribution, Kruskal-Wallis test with Dunn's multiple comparisons. Statistical differences between two different parameters were determined using one-way ANOVA with Tukey's multiple comparisons test. Statistical tests were performed using GraphPad Prism software (version 7), and differences were considered to be statistically significant at $p \leq 0.05$.

ACKNOWLEDGEMENTS
We thank the core staff at the UCL Cancer Institute Flow Cytometry Facility for sorting CRISPR/Cas9 edited FRC cell lines and for use of BD LSRFortessa X-20 flow cytometer. This work is supported by a Netherlands Organization for Scientific Research (NWO) Rubicon Postdoctoral Fellowship (019.162LW.004; to C.M.d.W), European Research Council Starting Grant (LNEXPANDS; to S.E.A), Cancer Research UK Career Development Fellowship (CRUK-A19763; to S.E.A) and Medical Research Council (MC-U12266B).

AUTHOR CONTRIBUTIONS CMdW and SEA designed the study and wrote the manuscript; SM performed *in vivo* protein expression analysis; LM investigated changes in and transcriptional control of podoplanin expression upon CLEC-2; ACB generated (inducible) PDPN-KO FRC cell lines and assisted with cell sorting; GC characterized CD82 KO FRC single cell clones and investigated podoplanin expression; VGM performed FRC transcriptome analysis and analysed podoplanin protein expression in the lymph node FRC network; CMdW generated CD44 KO, CD9 KO, CD44/CD9 DKO, and CD82 KO FRC cell lines, and performed and analysed all other experiments.

Bibliography

1. Miguel Quintanilla, Lucía Montero-Montero, Jaime Renart, Ester Martín-Villar, Miguel Quintanilla, Lucía Montero-Montero, Jaime Renart, and Ester Martín-Villar. Podoplanin in Inflammation and Cancer. *International Journal of Molecular Sciences*, 20(3):707, feb 2019. ISSN 1422-0067. doi: 10.3390/ijms20030707.
2. S Breiteneder-Geleff, K Matsui, A Soleiman, P Meraner, H Poczewski, R Kalt, G Schaffner, and D Kerjaschki. Podoplanin, novel 43-kd membrane protein of glomerular epithelial cells, is down-regulated in puromycin nephrosis. *The American journal of pathology*, 151(4): 1141–52, oct 1997. ISSN 0002-9440.
3. A. Wetterwald, W. Hofstetter, M.G. Cecchini, B. Lanske, C. Wagner, H. Fleisch, and M. Atkinson. Characterization and cloning of the E11 antigen, a marker expressed by Rat Osteoblasts and Osteocytes. *Bone*, 18(2):125–132, feb 1996. ISSN 8756-3282. doi: 10.1016/8756-3282(95)00457-2.
4. Miwa Tomooka, Chiaki Kaji, Hiroshi Kojima, and Yoshihiko Sawa. Distribution of podoplanin-expressing cells in the mouse nervous systems. *Acta histochemica et cytochemica*, 46(6): 171–7, dec 2013. ISSN 0044-5991. doi: 10.1267/ahc.13035.
5. Mary C Williams, Yu Xia Cao, Anne Hinds, Arun K Rishi, and Antoinette Wetterwald. T1α Protein Is Developmentally Regulated and Expressed by Alveolar Type I Cells, Choroid Plexus, and Ciliary Epithelia of Adult Rats. *American Journal of Respiratory Cell and Molecular Biology*, 14(6):577–585, dec 1996. ISSN 10441549. doi: 10.1165/ajrcmb.14.6.8652186.
6. Francisco G. Scholl, Carlos Gamallo, Senén Vilaró, and Miguel Quintanilla. Identification of PA2.26 antigen as a novel cell-surface mucin-type glycoprotein that induces plasma membrane extensions and increased motility in keratinocytes. *Journal of Cell Science*, 112(24): 4601–4613, 1999. ISSN 00219533.
7. A G Farr, M L Berry, A Kim, A J Nelson, M P Welch, and A Aruffo. Characterization and cloning of a novel glycoprotein expressed by stromal cells in T-dependent areas of peripheral lymphoid tissues. *The Journal of experimental medicine*, 176(5):1477–82, nov 1992. ISSN 0022-1007. doi: 10.1084/jem.176.5.1477.
8. Anna Karin H. Ekwall, Thomas Eisler, Christian Anderberg, Chunsheng Jin, Niclas Karlsson, Mikael Brisslert, and Maria I Bokarewa. The tumour-associated glycoprotein podoplanin is expressed in fibroblast-like synoviocytes of the hyperplastic synovial lining layer in rheumatoid arthritis. *Arthritis Research and Therapy*, 13(2):R40, mar 2011. ISSN 14786362. doi: 10.1186/ar3274.
9. Haruhisa Kitano, Shun Ichiro Kageyama, Stephen M. Hewitt, Ryuji Hayashi, Yoshinori Doki, Yoshitomo Ozaki, Shozo Fujino, Mikiko Takikita, Hajime Kubo, and Junya Fukuoka. Podoplanin expression in cancerous stroma induces lymphangiogenesis and predicts lymphatic spread and patient survival. *Archives of Pathology and Laboratory Medicine*, 134 (10):1520–1527, 2010. ISSN 00039985.
10. Edris A.F. Mahtab, Maurits C.E.F. Wijffels, Nynke M.S. Van Den Akker, Nathan D. Hahurij, Heleen Lie-Venema, Lambertus J. Wisse, Marco C. DeRuiter, Pavel Uhrin, Jan Zaujec, Bernd R. Binder, Martin J. Schalij, Robert E. Poelmann, and Adriana C. Gittenberger-De Groot. Cardiac malformations and myocardial abnormalities inpodoplanin knockout mouse embryos: Correlation with abnormal epicardial development. *Developmental Dynamics*, 237(3):847–857, mar 2008. ISSN 10588388. doi: 10.1002/dvdy.21463.
11. Edris A.F. Mahtab, Rebecca Vicente-Steijn, Nathan D. Hahurij, Monique R.M. Jongbloed, Lambertus J. Wisse, Marco C. DeRuiter, Pavel Uhrin, Jan Zaujec, Bernd R. Binder, Martin J. Schalij, Robert E. Poelmann, and Adriana C. Gittenberger-De Groot. Podoplanin deficient mice show a rhoa-related hypoplasia of the sinus venosus myocardium including the sinoatrial node. *Developmental Dynamics*, 238(1):183–193, jan 2009. ISSN 10588388. doi: 10.1002/dvdy.21819.
12. Maria I Ramirez, Guetchyn Millien, Anne Hinds, YuXia Cao, David C Seldin, and Mary C Williams. T1α, a lung type I cell differentiation gene, is required for normal lung cell proliferation and alveolus formation at birth. *Developmental Biology*, 256(1):62–73, apr 2003. ISSN 0012-1606. doi: 10.1016/S0012-1606(02)00098-2.
13. Vivien Schacht, Maria I. Ramirez, Young Kwon Hong, Satoshi Hirakawa, Dian Feng, Natasha Harvey, Mary Williams, Ann M. Dvorak, Harold F. Dvorak, Guillermo Oliver, and Michael Detmar. T1alpha/podoplanin deficiency disrupts normal lymphatic vasculature formation and causes lymphedema. *EMBO Journal*, 22(14):3546–3556, 2003. ISSN 02614189. doi: 10.1093/emboj/cdg342.
14. Katsue Suzuki-Inoue, Osamu Inoue, Guo Ding, Satoshi Nishimura, Kazuya Hokamura, Koji Eto, Hirokazu Kashiwagi, Yoshiaki Tomiyama, Yutaka Yatomi, Kazuo Umemura, Yonchol Shin, Masanori Hirashima, and Yukio Ozaki. Essential in vivo roles of the C-type lectin receptor CLEC-2: embryonic/neonatal lethality of CLEC-2-deficient mice by blood/lymphatic misconnections and impaired thrombus formation of CLEC-2-deficient platelets. *The Journal of biological chemistry*, 285(32):24494–507, aug 2010. ISSN 1083-351X. doi: 10.1074/jbc.M110.130575.
15. Masaru Honma, Masako Minami-Hori, Hidetoshi Takahashi, and Hajime Iizuka. Podoplanin expression in wound and hyperproliferative psoriatic epidermis: Regulation by TGF-β and STAT-3 activating cytokines, IFN-γ, IL-6, and IL-22. *Journal of Dermatological Science*, 65 (2):134–140, feb 2012. ISSN 0923-1811. doi: 10.1016/J.JDERMSCI.2011.11.011.
16. Jessica R. Hitchcock, Charlotte N. Cook, Saeeda Bobat, Ewan A. Ross, Adriana Flores-Langarica, Kate L. Lowe, Mahmood Khan, C. Coral Dominguez-Medina, Sian Lax, Manuela Carvalho-Gaspar, Stefan Hubscher, G. Ed Rainger, Mark Cobbold, Christopher D. Buckley, Tim J. Mitchell, Andrea Mitchell, Nick D. Jones, N. Van Rooijen, Daniel Kirchhofer, Ian R. Henderson, David H. Adams, Steve P. Watson, and Adam F. Cunningham. Inflammation drives thrombosis after Salmonella infection via CLEC-2 on platelets. *Journal of Clinical Investigation*, 125(12):4429–4446, 2015. ISSN 15588238. doi: 10.1172/JCI79070.
17. Jillian L Astarita, Sophie E Acton, and Shannon J Turley. Podoplanin: emerging functions in development, the immune system, and cancer. *Frontiers in immunology*, 3(September): 283, jan 2012. ISSN 1664-3224. doi: 10.3389/fimmu.2012.00283.

18. Chen-Ying Yang, Tobias K Vogt, Stéphanie Favre, Leonardo Scarpellino, Hsin-Ying Huang, Fabienne Tacchini-Cottier, and Sanjiv A Luther. Trapping of naive lymphocytes triggers rapid growth and remodeling of the fibroblast network in reactive murine lymph nodes. *Proceedings of the National Academy of Sciences of the United States of America*, 111(1):E109–18, 2014. ISSN 1091-6490. doi: 10.1073/pnas.1312585111.
19. Shubham Pandey, Frédéric Mourcin, Tony Marchand, Saba Nayar, Marion Guirriec, Céline Pangault, Céline Monvoisin, Patricia Amé-Thomas, Fabien Guilloton, Joelle Dulong, Mark Coles, Thierry Fest, Anja Mottok, Francesca Barone, and Karin Tarte. IL-4/CXCL12 loop is a key regulator of lymphoid stroma function in follicular lymphoma. *Blood*, 129(18):2507–2518, may 2017. ISSN 1528-0020. doi: 10.1182/blood-2016-08-737239.
20. Moritz Durchdewald, Juan Guinea-Viniegra, Daniel Haag, Astrid Riehl, Peter Lichter, Meinhard Hahn, Erwin F Wagner, Peter Angel, and Jochen Hess. Podoplanin is a novel fos target gene in skin carcinogenesis. *Cancer Research*, 68(17):6877–6883, sep 2008. ISSN 00085472. doi: 10.1158/0008-5472.CAN-08-0299.
21. Akiko Kunita, Takeshi G. Kashima, Atsushi Ohazama, Agamemnon E. Grigoriadis, and Masashi Fukayama. Podoplanin Is Regulated by AP-1 and Promotes Platelet Aggregation and Cell Migration in Osteosarcoma. *The American Journal of Pathology*, 179(2):1041–1049, aug 2011. ISSN 0002-9440. doi: 10.1016/J.AJPATH.2011.04.027.
22. Heike Peterziel, Julia Müller, Andreas Danner, Sebastian Barbus, Hai Kun Liu, Bernhard Radlwimmer, Torsten Pietsch, Peter Lichter, Günther Schütz, Jochen Hess, and Peter Angel. Expression of podoplanin in human astrocytic brain tumors is controlled by the PI3K-AKT-AP-1 signaling pathway and promoter methylation. *Neuro-Oncology*, 14(4):426–439, apr 2012. ISSN 15228517. doi: 10.1093/neuonc/nos055.
23. Young-Kwon Hong, Natasha Harvey, Yun-Hee Noh, Vivien Schacht, Satoshi Hirakawa, Michael Detmar, and Guillermo Oliver. Prox1 is a master control gene in the program specifying lymphatic endothelial cell fate. *Developmental Dynamics*, 225(3):351–357, nov 2002. ISSN 1058-8388. doi: 10.1002/dvdy.10163.
24. Sophie E. Acton, Aaron J. Farrugia, Jillian L. Astarita, Diego Mourão-Sá, Robert P. Jenkins, Emma Nye, Steven Hooper, Janneke van Blijswijk, Neil C. Rogers, Kathryn J. Snelgrove, Ian Rosewell, Luis F. Moita, Gordon Stamp, Shannon J. Turley, Erik Sahai, and Caetano Reis e Sousa. Dendritic cells control fibroblastic reticular network tension and lymph node expansion. *Nature*, 514(7523):498–502, oct 2014. ISSN 0028-0836. doi: 10.1038/nature13814.
25. Jillian L Astarita, Viviana Cremasco, Jianxin Fu, Max C Darnell, James R Peck, Janice M Nieves-Bonilla, Kai Song, Yuji Kondo, Matthew C Woodruff, Alvin Gogineni, Lucas Onder, Burkhard Ludewig, Robby M Weimer, Michael C Carroll, David J Mooney, Lijun Xia, and Shannon J Turley. The CLEC-2-podoplanin axis controls the contractility of fibroblastic reticular cells and lymph node microarchitecture. *Nature immunology*, 16(1):75–84, 2015. ISSN 1529-2916. doi: 10.1038/ni.3035.
26. Brett H Herzog, Jianxin Fu, Stephen J Wilson, Paul R Hess, Aslihan Sen, J. Michael McDaniel, Yanfang Pan, Minjia Sheng, Tadayuki Yago, Robert Silasi-Mansat, Samuel McGee, Frauke May, Bernhard Nieswandt, Andrew J Morris, Florea Lupu, Shaun R Coughlin, Rodger P. McEver, Hong Chen, Mark L Kahn, and Lijun Xia. Podoplanin maintains high endothelial venule integrity by interacting with platelet CLEC-2. *Nature*, 502(7469):105–9, oct 2013. ISSN 1476-4687. doi: 10.1038/nature12501.
27. Cécile Bénézech, Saba Nayar, Brenda a. Finney, David R. Withers, Kate Lowe, Guillaume E. Desanti, Clare L. Marriott, Steve P. Watson, Jorge H. Caamaño, Christopher D. Buckley, and Francesca Barone. CLEC-2 is required for development and maintenance of lymph nodes. *Blood*, 123:3200–3207, 2014. ISSN 15280020. doi: 10.1182/blood-2013-03-489286.
28. Leah N. Cueni and Michael Detmar. Galectin-8 interacts with podoplanin and modulates lymphatic endothelial cell functions. *Experimental Cell Research*, 315(10):1715–1723, jun 2009. ISSN 0014-4827. doi: 10.1016/J.YEXCR.2009.02.021.
29. Takashi Shibuya, Masaru Honma, Mizue Fujii, Shin Iinuma, and Akemi Ishida-Yamamoto. Podoplanin suppresses the cell adhesion of epidermal keratinocytes via functional regulation of β1-integrin. *Archives of Dermatological Research*, 311(1):45–53, nov 2019. ISSN 1432069X. doi: 10.1007/s00403-018-1878-9.
30. Lewis S C Ward, Lozan Sheriff, Jennifer L Marshall, Julia E Manning, Alexander Brill, Gerard B Nash, and Helen M McGettrick. Podoplanin regulates the migration of mesenchymal stromal cells and their interaction with platelets. *Journal of cell science*, 132(5):jcs.222067, feb 2019. ISSN 1477-9137. doi: 10.1242/jcs.222067.
31. Jaroslaw Suchanski, Anna Tejchman, Maciej Zacharski, Aleksandra Piotrowska, Jedrzej Grzegrzolka, Grzegorz Chodaczek, Katarzyna Nowinska, Janusz Rys, Piotr Dziegiel, Claudine Kieda, and Maciej Ugorski. Podoplanin increases the migration of human fibroblasts and affects the endothelial cell network formation: A possible role for cancer-associated fibroblasts in breast cancer progression. *PLOS ONE*, 12(9):e0184970, sep 2017. ISSN 1932-6203. doi: 10.1371/journal.pone.0184970.
32. Andreas Wicki, François Lehembre, Nikolaus Wick, Brigitte Hantusch, Dontscho Kerjaschki, and Gerhard Christofori. Tumor invasion in the absence of epithelial-mesenchymal transition: Podoplanin-mediated remodeling of the actin cytoskeleton. *Cancer Cell*, 9(4):261–272, 2006. ISSN 15356108. doi: 10.1016/j.ccr.2006.03.010.
33. E Martín-Villar, B Fernández-Muñoz, M Parsons, MM Yurrita, D Megías, E Pérez-Gómez, GE Jones, and M Quintanilla. Podoplanin Associates with CD44 to Promote Directional Cell Migration. *Mol Biol Cell*, 21(24):4387–99, 2010. doi: 10.1091/mbc.E10-06-0489.
34. Akiko Kunita, Vanessa Baeriswyl, Claudia Meda, Erik Cabuy, Kimiko Takeshita, Enrico Giraudo, Andreas Wicki, Masashi Fukayama, and Gerhard Christofori. Inflammatory Cytokines Induce Podoplanin Expression at the Tumor Invasive Front. *American Journal of Pathology*, 188(5):1276–1288, feb 2018. ISSN 15252191. doi: 10.1016/j.ajpath.2018.01.016.
35. E Martín-Villar, B Borda-d'Agua, P Carrasco-Ramirez, J Renart, M Parsons, M Quintanilla, and G E Jones. Podoplanin mediates ECM degradation by squamous carcinoma cells through control of invadopodia stability. *Oncogene*, 34(October):4531–4544, aug 2015. ISSN 1476-5594. doi: 10.1038/onc.2014.388.
36. Ester Martín-Villar, Diego Megías, Susanna Castel, Maria Marta Yurrita, Senén Vilaró, and Miguel Quintanilla. Podoplanin binds ERM proteins to activate RhoA and promote epithelial-mesenchymal transition. *Journal of Cell Science*, 119(21):4541–4553, 2006. doi: 10.1242/jcs.03218.
37. Ester Martín-Villar, Francisco G. Scholl, Carlos Gamallo, Maria M. Yurrita, Mario Muñoz-Guerra, Jesús Cruces, and Miguel Quintanilla. Characterization of human PA2.26 antigen (T1α-2, podoplanin), a small membrane mucin induced in oral squamous cell carcinomas. *International Journal of Cancer*, 113(6):899–910, mar 2005. ISSN 00207136. doi: 10.1002/ijc.20656.
38. Sjoerd J. van Deventer, Vera Marie E Dunlock, and Annemiek B. van Spriel. Molecular interactions shaping the tetraspanin web. *Biochemical Society Transactions*, 45(3):741–750, 2017. ISSN 0300-5127. doi: 10.1042/BST20160284.
39. Christina M. Termini and Jennifer M. Gillette. Tetraspanins Function as Regulators of Cellular Signaling. *Frontiers in cell and developmental biology*, 5:34, apr 2017. ISSN 2296-634X. doi: 10.3389/fcell.2017.00034.
40. Youya Nakazawa, Shigeo Sato, Mikihiko Naito, Yukinari Kato, Kazuhiko Mishima, Hiroyuki Arai, Takashi Tsuruo, and Naoya Fujita. Tetraspanin family member CD9 inhibits Aggrus/podoplanin-induced platelet aggregation and suppresses pulmonary metastasis. *Blood*, 112(5):1730–1739, 2008. ISSN 00064971. doi: 10.1182/blood-2007-11-124693.
41. Beatriz Fernández-Muñoz, María M. Yurrita, Ester Martín-Villar, Patricia Carrasco-Ramírez, Diego Megías, Jaime Renart, and Miguel Quintanilla. The transmembrane domain of podoplanin is required for its association with lipid rafts and the induction of epithelial-mesenchymal transition. *International Journal of Biochemistry and Cell Biology*, 43(6):886–896, 2011. ISSN 13572725. doi: 10.1016/j.biocel.2011.02.010.
42. Lucie Peduto, Sophie Dulauroy, Matthias Lochner, Gerald F Späth, Miguel A Morales, Ana Cumano, and Gérard Eberl. Inflammation recapitulates the ontogeny of lymphoid stromal cells. *Journal of immunology (Baltimore, Md. : 1950)*, 182(9):5789–99, may 2009. ISSN 1550-6606. doi: 10.4049/jimmunol.0803974.
43. Victor G Martinez, Valeriya Pankova, Lukas Krasny, Tanya Singh, Ian J. White, Agnesska C. Benjamin, Simone Dertschnig, Harry L. Horsnell, Janos Kriston-Vizi, Jemima J. Burden, Paul H. Huang, Christopher J. Tape, and Sophie Acton. Conduit Integrity is Compromised During Acute Lymph Node Expansion. *bioRxiv*, page 527481, jan 2019. doi: 10.2139/ssrn.3334979.
44. F Berditchevski and E Odintsova. Tetraspanins as regulators of protein trafficking. *Traffic*, 8 (2):89–96, 2007.
45. Alexis Bergsma, Sourik S. Ganguly, Mollie E. Wiegand, Daniel Dick, Bart O. Williams, and Cindy K. Miranti. Regulation of cytoskeleton and adhesion signaling in osteoclasts by tetraspanin CD82. *Bone Reports*, 10:100196, jun 2019. ISSN 23521872. doi: 10.1016/j.bonr.2019.100196.
46. Brandon Zimmerman, Brian McMillan, Tom Seegar, Andrew Kruse, and Stephen Blacklow. Crystal Structure of Human Tetraspanin CD81 Reveals a Conserved Intramembrane Binding Cavity. *The FASEB Journal*, 30(1 Supplement):lb71–lb71, 2016. ISSN 0892-6638. doi: 10.1016/j.cell.2016.09.056.
47. Sophie E Acton, Jillian L Astarita, Deepali Malhotra, Veronika Lukacs-Kornek, Bettina Franz, Paul R Hess, Zoltan Jakus, Michael Kuligowski, Anne L Fletcher, Kutlu G Elpek, Angelique Bellemare-Pelletier, Lindsay Sceats, Erika D Reynoso, Santiago F Gonzalez, Daniel B Graham, Jonathan Chang, Anneli Peters, Matthew Woodruff, Young-A Kim, Wojciech Swat, Takashi Morita, Vijay Kuchroo, Michael C Carroll, Mark L Kahn, Kai W Wucherpfennig, and Shannon J Turley. Podoplanin-rich stromal networks induce dendritic cell motility via activation of the C-type lectin receptor CLEC-2. *Immunity*, 37(2):276–89, aug 2012. ISSN 1097-4180. doi: 10.1016/j.immuni.2012.05.022.
48. Diego Mourão-Sá, Matthew J Robinson, Santiago Zelenay, David Sancho, Probir Chakravarty, Rasmus Larsen, Maud Plantinga, Nico Van Rooijen, Miguel P Soares, Bart Lambrecht, Caetano Reis e Sousa, Diego Moura, David Sancho, Probir Chakravarty, Rasmus Larsen, Maud Plantinga, Nico Van Rooijen, Miguel P Soares, and Bart Lambrecht. CLEC-2 signaling via Syk in myeloid cells can regulate inflammatory responses. *European journal of immunology*, 41(10):3040–53, oct 2011. ISSN 1521-4141. doi: 10.1002/eji.201141641.
49. Charlotte M de Winde, Alexandra L Matthews, Sjoerd van Deventer, Alie van der Schaaf, Neil D Tomlinson, Jing Yang, Erik Jansen, Johannes A Eble, Bernhard Nieswandt, Helen M McGettrick, Carl G Figdor, Sophie E Acton, Michael G Tomlinson, and Annemiek B van Spriel. C-type lectin-like receptor 2 (CLEC-2)-dependent DC migration is controlled by tetraspanin CD37. *Journal of cell science*, 131(19):jcs214551, sep 2018. doi: 10.1242/jcs.214551.
50. Klemens Rottner and Matthias Schaks. Assembling actin filaments for protrusion. *Current Opinion in Cell Biology*, 56:53–63, feb 2019. ISSN 0955-0674. doi: 10.1016/J.CEB.2018.09.004.
51. Keisuke Kaji, Shoji Oda, Tomohide Shikano, Tatsuya Ohnuki, Yoshikatsu Uematsu, Junko Sakagami, Norihiro Tada, Shunichi Miyazaki, and Akira Kudo. The gamete fusion process is defective in eggs of Cd9-deficient mice. *Nature Genetics*, 24(3):279–282, mar 2000. ISSN 1061-4036. doi: 10.1038/73502.
52. Raquel Reyes, Beatriz Cardeñes, Yesenia Machado-Pineda, and Carlos Cabañas. Tetraspanin CD9: A key regulator of cell adhesion in the immune system, apr 2018. ISSN 16643224.
53. Anne L Fletcher, Sophie E Acton, and Konstantin Knoblich. Lymph node fibroblastic reticular cells in health and disease. *Nature reviews. Immunology*, 15(6):350–361, 2015. ISSN 1474-1741. doi: 10.1038/nri3846.
54. Lauren B Rodda, Erick Lu, Mariko L Bennett, Caroline L Sokol, Xiaoming Wang, Sanjiv A Luther, Ben A Barres, Andrew D Luster, Chun Jimmie Ye, and Jason G Cyster. Single-Cell RNA Sequencing of Lymph Node Stromal Cells Reveals Niche-Associated Heterogeneity. *Immunity*, 48(5):1014–1028.e6, apr 2018. ISSN 1097-4180. doi: 10.1016/j.immuni.2018.04.006.
55. Tomoya Katakai, Hidenori Suto, Manabu Sugai, Hiroyuki Gonda, Atsushi Togawa, Sachiko Suematsu, Yukihiko Ebisuno, Koko Katagiri, Tatsuo Kinashi, and Akira Shimizu. Organizer-like reticular stromal cell layer common to adult secondary lymphoid organs. *Journal of immunology (Baltimore, Md. : 1950)*, 181(9):6189–200, nov 2008. ISSN 1550-6606. doi: 10.4049/jimmunol.181.9.6189.
56. Marc Bajénoff and Ronald N. Germain. B-cell follicle development remodels the conduit system and allows soluble antigen delivery to follicular dendritic cells. *Blood*, 114(24):4989–4997, dec 2009. ISSN 0006-4971. doi: 10.1182/BLOOD-2009-06-229567.
57. Ramon Roozendaal, Thorsten R Mempel, Lisa a Pitcher, F Santiago, Admar Verschoor, Reina E Mebius, Ulrich H Von Andrian, and C Michael. Conduits Mediate Transport of Low

Molecular Weight Antigen to Lymph Node Follicles. *Immunity*, 30(2):264–276, 2010. doi: 10.1016/j.immuni.2008.12.014.Conduits.

58. Di Huang, Jianing Chen, Linbin Yang, Qian Ouyang, Jiaqian Li, Liyan Lao, Jinghua Zhao, Jiang Liu, Yiwen Lu, Yue Xing, Fei Chen, Fengxi Su, Herui Yao, Qiang Liu, Shicheng Su, and Erwei Song. NKILA lncRNA promotes tumor immune evasion by sensitizing T cells to activation-induced cell death. *Nature Immunology*, 19(10):1112–1125, oct 2018. ISSN 15292916. doi: 10.1038/s41590-018-0207-y.
59. Isabelle Mondor, Myriam Baratin, Marine Lagueyrie, Lisa Saro, Sandrine Henri, Rebecca Gentek, Delphine Suerinck, Wolfgang Kastenmuller, Jean X Jiang, and Marc Bajénoff. Lymphatic Endothelial Cells Are Essential Components of the Subcapsular Sinus Macrophage Niche. *Immunity*, 50(6):1453–1466.e4, apr 2019. ISSN 10974180. doi: 10.1016/j.immuni.2019.04.002.
60. Abdouramane Camara, Olga G Cordeiro, Farouk Alloush, Janina Sponsel, Mélanie Chypre, Lucas Onder, Kenichi Asano, Masato Tanaka, Hideo Yagita, Burkhard Ludewig, Vincent Flacher, and Christopher G Mueller. Lymph Node Mesenchymal and Endothelial Stromal Cells Cooperate via the RANK-RANKL Cytokine Axis to Shape the Sinusoidal Macrophage Niche. *Immunity*, 50(6):1467–1481.e6, jun 2019. ISSN 1097-4180. doi: 10.1016/j.immuni.2019.05.008.
61. Tomoya Katakai. Marginal reticular cells: a stromal subset directly descended from the lymphoid tissue organizer. *Frontiers in immunology*, 3:200, 2012. ISSN 1664-3224. doi: 10.3389/fimmu.2012.00200.
62. Spyridon Makris and Sophie E. Acton. The Stromal Niche Guarding the Gatekeepers. *Immunity*, 50(6):1344–1346, jun 2019. ISSN 1074-7613. doi: 10.1016/J.IMMUNI.2019.05.019.
63. Mario Novkovic, Lucas Onder, Jovana Cupovic, Jun Abe, David Bomze, Viviana Cremasco, Elke Scandella, Jens V. Stein, Gennady Bocharov, Shannon J. Turley, and Burkhard Ludewig. Topological Small-World Organization of the Fibroblastic Reticular Cell Network Determines Lymph Node Functionality. *PLOS Biology*, 14(7):e1002515, jul 2016. ISSN 1545-7885. doi: 10.1371/journal.pbio.1002515.
64. Kasper M W Soekarjo, Johannes Textor, and Rob J de Boer. Local Attachment Explains Small World–like Properties of Fibroblastic Reticular Cell Networks in Lymph Nodes. *The Journal of Immunology*, 202(11):3318–3325, apr 2019. ISSN 0022-1767. doi: 10.4049/jimmunol.1801016.
65. Xupin Jiang, Jiaping Zhang, and Yuesheng Huang. Tetraspanins in cell migration. *Cell Adhesion and Migration*, 9(5):406–415, 2015. ISSN 19336926. doi: 10.1080/19336918.2015.1005465.
66. S Tsukita, K Oishi, N Sato, J Sagara, A Kawai, and S Tsukita. ERM family members as molecular linkers between the cell surface glycoprotein CD44 and actin-based cytoskeletons. *The Journal of cell biology*, 126(2):391–401, jul 1994. ISSN 0021-9525. doi: 10.1083/jcb.126.2.391.
67. Marco B. Schaaf, Abhishek D. Garg, and Patrizia Agostinis. Defining the role of the tumor vasculature in antitumor immunity and immunotherapy article, feb 2018. ISSN 20414889.
68. Elena Neumann, Maria C Schwarz, Rebecca Hasseli, Marie-Lisa Hülser, Simon Classen, Michael Sauerbier, Stefan Rehart, and Ulf Mueller-Ladner. Tetraspanin CD82 affects migration, attachment and invasion of rheumatoid arthritis synovial fibroblasts. *Annals of the rheumatic diseases*, 77(11):1619–1626, nov 2018. ISSN 1468-2060. doi: 10.1136/annrheumdis-2018-212954.

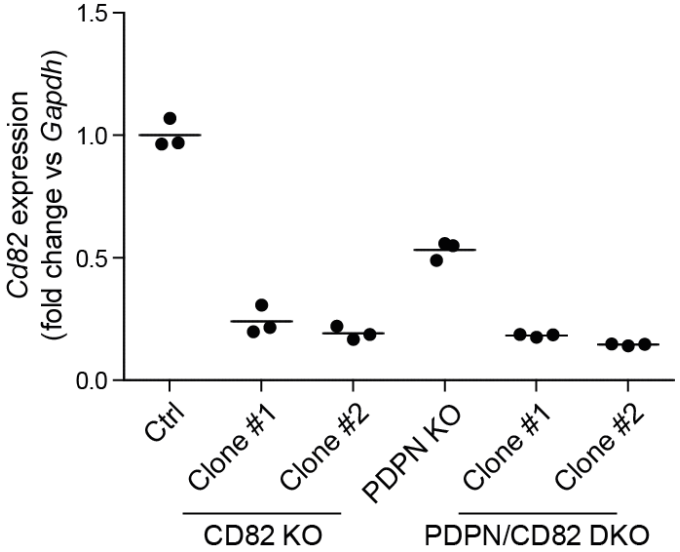

Fig. S1. Validation of CD82 knock-out FRC clones. Two single clones of CD82 knock-out (KO) and PDPN/CD82 double-KO (DKO) FRCs were validated using *Cd82* mRNA expression by lack of a good CD82 antibody for flow cytometry. *Cd82* mRNA expression is calculated as fold change of *Gapdh* expression. Three technical replicates for each cell line, and representative data from two independent experiments is shown.

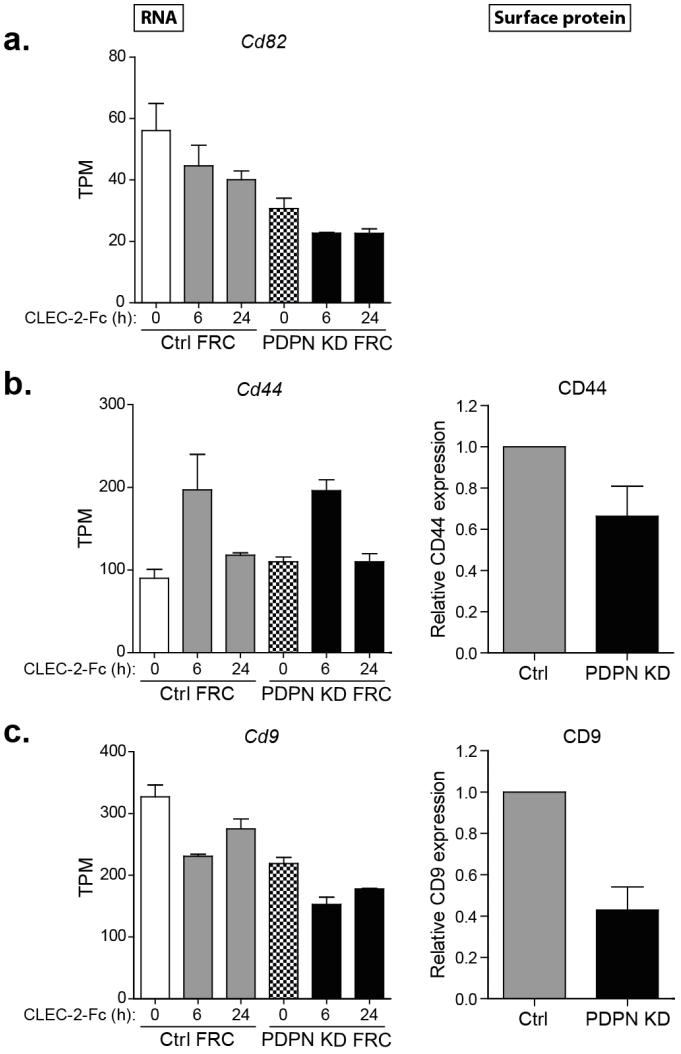

Fig. S2. CD82, CD44 and CD9 expression correlates with podoplanin expression. CD82 (**a**), CD44 (**b**) and CD9 (**c**) mRNA (left; RNA sequencing) and surface protein (right; flow cytometry) expression in control (Ctrl) and podoplanin siRNA knock-down (PDPN KD) FRC cell lines. For RNA sequencing, FRCs were treated for 6 or 24 hours with CLEC-2-Fc. TPM, transcripts per million.